

Published in final edited form as:

Med. 2021 November 12; 2(11): 1231–1252.e10. doi:10.1016/j.medj.2021.10.002.

LRG1 destabilizes tumor vessels and restricts immunotherapeutic potency

Marie N. O'Connor^{1,‡}, David M. Kallenberg^{1,‡}, Carlotta Camilli¹, Camilla Pilotti¹, Athina Dritsoula¹, Rene Jackstadt², Chantelle E. Bowers¹, H. Angharad Watson¹, Markella Alatsatianos³, Julia Ohme³, Laura Dowsett¹, Jestin George¹, Jack W.D. Blackburn¹, Xiaomeng Wang¹, Mahak Singhal^{4,5}, Hellmut G. Augustin^{4,5}, Ann Ager³, Owen J. Sansom^{2,6}, Stephen E. Moss^{*,†,1}, John Greenwood^{*,†,1}

¹Institute of Ophthalmology, University College London, London, SE5 8BN, UK

²Cancer Research UK Beatson Institute, Glasgow, G61 1BD, UK

³Division of Infection and Immunity, School of Medicine and Systems Immunity University Research Institute, Cardiff University, Cardiff, CF14 4XN, UK

⁴Division of Vascular Oncology and Metastasis, German Cancer Research Center (DKFZ- ZMBH Alliance), Heidelberg, Germany

⁵Department of Vascular Biology and Tumor Angiogenesis, European Center for Angioscience (ECAS), Medical Faculty Mannheim, Heidelberg University, Mannheim, Germany

⁶Institute of Cancer Sciences, University of Glasgow, Glasgow, G61 1QH, UK

Summary

Background—A poorly functioning tumor vasculature is pro-oncogenic and may impede the delivery of therapeutics. Normalizing the vasculature, therefore, may be beneficial. We previously reported that the secreted glycoprotein leucine-rich a-2-glycoprotein 1 (LRG1) contributes to

*Correspondence: j.greenwood@ucl.ac.uk (J.G.) or s.moss@ucl.ac.uk (S.E.M.).

‡These authors contributed equally

†These authors contributed equally

Author Contribution

J.G. and S.E.M. conceived, designed, and directed the overall study and had unrestricted access to all of the data. A.A. and H.A.W. designed the adoptive T cell experiments, and O.J.S. and R.J. designed the genetically engineered mouse model experiments. X.W. undertook the initial B16-F0 experiment. M.N.O., D.M.K., C.C., C.P., C.E.B., and J.W.D.B. performed all of the subsequent experimental work using the B16-F0 and LLC models. R.J., O.J.S., and M.N.O. conducted and analyzed the experimental work using the genetic cancer models. M.N.O., D.M.K., C.P., C.C., L.D., and C.E.B. undertook the histological staining and analysis using the B16F0 and LLC model. M.N.O. and C.C. carried out the RNAScope in situ hybridization analysis. H.A.W., M.A., and J.O. conducted the adoptive T cell experiments. M.N.O., D.M.K., C.C., and C.P. performed the analysis of immune cell infiltration into tumors. L.D. and A.D. undertook the gene analysis studies. C.E.B. and J.W.D.B. carried out the human LRG1 ELISA analysis. M.S. and H.G.A. designed and undertook the mouse metastasis work. M.N.O. oversaw all of the statistical analyses. J. George and J.W.D.B. generated and purified the 15C4 blocking antibody. J.G. and S.E.M. prepared the first draft of the manuscript, reviewed it, and edited it, with input from M.N.O., D.M.K., and C.C., and collaborators A.A., R.J., O.J.S., M.S., and H.G.A. All of the authors contributed and agreed to submission of the manuscript. All of the authors have read and approved the final draft and take full responsibility for its content, including the accuracy of the data and their statistical analysis.

Declaration of Interests

J.G. and S.E.M. are founders of a company spun out by UCL Business to commercialize a LRG1 function-blocking therapeutic antibody developed through the UK Medical Research Council DPFS funding scheme. This is currently directed towards treating ocular disease. J.G. and S.E.M. are members of the scientific advisory board and are shareholders of this company and named inventors on three patents related to LRG1 as a therapeutic target.

pathogenic neovascularization. Here, we investigate whether LRG1 in tumors is vasculopathic and whether its inhibition has therapeutic utility.

Methods—Tumor growth and vascular structure were analyzed in subcutaneous and genetically engineered mouse models in wild-type and *Lrg1* knockout mice. The effects of LRG1 antibody blockade as monotherapy, or in combination with co-therapies, on vascular function, tumor growth, and infiltrated lymphocytes were investigated.

Findings—In mouse models of cancer, *Lrg1* expression was induced in tumor endothelial cells, consistent with an increase in protein expression in human cancers. The expression of LRG1 affected tumor progression as *Lrg1* gene deletion, or treatment with a LRG1 function-blocking antibody, inhibited tumor growth and improved survival. Inhibition of LRG1 increased endothelial cell pericyte coverage and improved vascular function, resulting in enhanced efficacy of cisplatin chemotherapy, adoptive T cell therapy, and immune checkpoint inhibition (anti-PD1) therapy. With immunotherapy, LRG1 inhibition led to a significant shift in the tumor microenvironment from being predominantly immune silent to immune active.

Conclusions—LRG1 drives vascular abnormalization, and its inhibition represents a novel and effective means of improving the efficacy of cancer therapeutics.

Funding—Wellcome Trust (206413/B/17/Z), UKRI/MRC (G1000466, MR/N006410/1, MC/PC/14118, and MR/L008742/1), BHF (PG/16/50/32182), Health and Care Research Wales (CA05), CRUK (C42412/A24416 and A17196), ERC (ColonCan 311301 and AngioMature 787181), and DFG (CRC1366).

Introduction

Angiogenesis is notably different in development and disease, with the former producing an organized, stable, and functional vascular network, and the latter being typically disorganized and dysfunctional. However, vascularization in both settings is driven by many of the same molecules, such as vascular endothelial growth factor (VEGF). Why vessels fail to grow in a patterned and functional manner in most disease settings remains poorly understood but points to the potential involvement of novel pathogenic factors that corrupt physiological angiogenesis. We, and others, have previously shown that in vascular pathology of the retina¹ and kidney², the secreted glycoprotein LRG1 is induced and promotes dysfunctional vessel growth through modifying endothelial cell transforming growth factor b (TGF- β) signaling. Importantly, the deletion of *Lrg1* in mice did not affect developmental angiogenesis, with the mice exhibiting no overt phenotype¹. These observations suggest that in disease, LRG1 may be a contributing pathogenic factor responsible for preventing the development of physiological vessels and thus play a role in the vascular dysfunction that is prevalent in cancer.

The formation of new blood vessels has long been recognized as an essential feature of tumor expansion, survival, and metastatic spread^{3,4}. Consequently, targeting of key pro-angiogenic signaling molecules, most notably VEGF through blocking antibodies such as bevacizumab, to limit vascular growth or to regress existing vessels has become an established therapeutic regimen. While such approaches have met with some success, resulting in an increase in progression-free survival in certain cancers, they have had little

impact on overall survival rate. As in other diseases, the cardinal features of tumor vessels are that they are poorly perfused, leaky, and hemorrhagic, characteristics believed to be due in part to the failure of vessel maturation. These abnormal features result in a hypoxic pro-oncogenic tumor microenvironment (TME) that promotes malignancy and metastatic spread, impairs beneficial immune responses, and limits the efficacy of systemically administered drugs and immunotherapeutics^{5,6}. Counter to the original rationale of blocking neovascularization, therefore, an alternative strategy has emerged that aims to normalize the vasculature and render the microenvironment more conducive to tumor destruction^{7,8}. In pursuit of this objective, various approaches have been tested, including the use of anti-VEGF drugs delivered at a lower dose than that required to prevent or ablate neovascularization⁹. This tactic has led to some improvement in the delivery of cancer therapeutics^{10,11}, but the timing and dosage remain problematic, especially as the window of opportunity with anti-VEGF drugs may be transient^{10,12,13}. To overcome this limitation, other vascular modifying approaches have been explored, either as monotherapy or in conjunction with existing anti-VEGF drugs^{14–22}. These studies have demonstrated that sustained vascular normalization can be achieved, at least in the experimental setting, and validate the potential utility of these strategies in enhancing the efficacy of the current standard of care and emerging treatments. Moreover, these studies also highlight the importance of crosstalk between the vasculature and the immune system in establishing a favorable therapeutic milieu^{19,23–26}. In particular, it has been shown that vascular normalization strategies combined with checkpoint inhibition result in the formation of high endothelial venule (HEV) characteristics within the tumor vasculature that help promote the recruitment of effector T cells¹⁴. It is clear, therefore, that there is much that we still need to understand about the contribution that the vasculature makes to tumor progression, and in so doing, reveal new potential therapeutic targets.

The discovery that LRG1 is associated with abnormal vessel growth in various diseases^{1,2} raises the possibility that this secreted glycoprotein contributes to abnormal tumor vessel growth. Consistent with this hypothesis, studies have shown LRG1 to be induced in many carcinomas, and there is growing evidence that raised blood LRG1 levels alone, or in combination with other biomarkers, correlate with increased tumor load and poor prognosis^{27–39}. Such data strongly implicate LRG1 in the pathogenesis of cancer and provide a rationale for further investigation. In this study, therefore, we aimed to establish whether LRG1 affects tumor vessel structure and function and crucially the implications of this on therapy. We show that LRG1 affects vessel growth, structure, and function, establishing it as a significant vascular destabilizing factor. By deleting *Lrg1*, or blocking its function with a targeted antibody, we observe reduced tumor growth and demonstrate that tumor vessels exhibit a more physiological configuration with improved pericyte coverage. The ramifications of vessel normalization brought about by LRG1 blockade were further investigated and revealed enhanced efficacy when combined with cytotoxic and immunotherapeutic strategies. These data provide evidence that the blockade of LRG1 in cancer offers a novel approach to vascular normalization, and in doing so, potentiates the efficacy of current and emerging therapies.

Results

LRG1 expression is increased in human cancer patients

Under normal conditions, LRG1 is expressed predominantly by the liver, but in cancer there is strong evidence that its expression is significantly induced^{27–39}. To confirm these findings, LRG1 protein was examined by immunohistochemistry in human lung, prostate, and breast carcinomas, with all three exhibiting high expression compared to adjacent normal appearing tissue or normal control tissue (Figures 1A–1C). We also observed expression of LRG1 in peritumoral endothelial cells (Figure 1D). Having corroborated tumor expression of LRG1, we next determined, as previously reported, whether various cancer types were also associated with raised circulating blood levels. In serum collected from treatment-naïve patients with grade III and above colorectal adenocarcinoma, pancreatic adenocarcinoma, and non-small cell lung carcinoma (squamous cell lung carcinoma), circulating levels of LRG1 were found to be significantly increased above normal circulating levels (Figure 1E). These data support the prevailing view that LRG1 may contribute to tumor progression.

Lrg1 deletion reduces experimental tumor growth and increases survival

To complement the data on LRG1 expression in human cancer, we next examined *Lrg1* expression in the syngeneic B16-F0 mouse melanoma and Lewis lung carcinoma (LLC) subcutaneous graft models, the KPC model of pancreatic ductal adenocarcinoma (PDAC) (*LSL-Kras*^{G12D/+}, *LSL-Trp53*^{R172H/+}, *Pdx-1-Cre*), and the *Apc*^{Min/+} and the *vil*^{CreER} *Apc*^{fl/+} models of colorectal cancer (CRC). *Lrg1* transcript was detected within the tumors of all of the models (Figures 1F–1H). In B16-F0 and LLC tumors, *Lrg1* expression appeared to be restricted mostly to vessels (Figure 1F), whereas in intestinal adenomas and PDAC, *Lrg1* expression was also highly upregulated in the neoplasm compared to normal tissue (Figures 1G, 1H, S1A, and S1B). Consistent throughout the different cancer models, *Lrg1*, which is not detectable in normal blood vessels, was induced in endothelial cells but not observed in α -smooth muscle actin (α -SMA⁺) perivascular mural cells (Figure 1I). We next investigated whether *Lrg1* gene expression was also increased in metastatic tumor vessels. Vessels from LLC lung metastases (Figure S1C) exhibited a strong induction of *Lrg1* compared with normal lung vessels in which the expression was barely detectable (Figures 1J and S1D). Overall, these observations align with our human data and previous reports,^{27–39} and raise the possibility that local secretion of LRG1 may affect the TME of primary and metastatic tumors and, in particular, through both autocrine and paracrine signaling, vascular function.

Our previous work demonstrated that *Lrg1* knockout (KO), or functional blockade with an antibody, reduced the size of neovascular lesions in models of age-related macular degeneration and ocular hypoxia¹. We therefore examined the effects of *Lrg1* gene deletion on tumor growth and survival across a range of syngeneic and genetic models. In the B16-F0 and LLC subcutaneous tumors, tumor growth was significantly reduced in *Lrg1*^{-/-} mice compared to wild-type (WT) controls (Figures 2A, 2B, S2A, and S2B), with a decrease in final tumor volume at the termination endpoints of 44% and 46%, respectively. Consistent with these observations, the *Apc*^{Min/+} (Figure 2C) and *vil*^{CreER} *Apc*^{fl/+} (Figure 2D) mice also exhibited a significantly enhanced survival rate on the *Lrg1*^{-/-} background. In both

colorectal models, there was a trend toward a reduced tumor number in *Lrg1*^{-/-} mice that reached significance in the colon and small intestine in the *Apc*^{Min/+} and *vil*^{CreER} *Apc*^{fl/+} mice, respectively (Figures 2E and 2F). We next investigated whether knockout of *Lrg1* affected the survival of KPC PDAC tumor-bearing mice⁴⁰. As with the other models, *Lrg1*^{-/-} KPC mice exhibited a significantly enhanced survival rate compared to *Lrg1*^{+/+} mice (Figure 2G). These results demonstrate that the deletion of *Lrg1*^{-/-} in a number of different tumor models improves outcomes and supports the hypothesis that LRG1 is pro-oncogenic.

***Lrg1* deletion results in tumor vessel normalization**

To ascertain whether reduced tumor size and enhanced survival in *Lrg1*^{-/-} mice correlated with changes in vascularization, we measured the percentage of vessel area in each tumor type. No difference in total vessel area between wild-type (WT) and *Lrg1* KO mice was observed across the different models (Figures 3A, 3B, and S2C). There was only a modest reduction in the number of vessel profiles per unit area in the B16-F0, LLC, and KPC mice on the *Lrg1*^{-/-} background, but a striking increase in the size of individual vessels (Figures 3B and 3C). Due to the planar orientation of the tumor vasculature in the *Apc*^{Min/+} models, comparable analysis of vessel density was not possible. Nonetheless, our observations that endothelial cells express the *Lrg1* gene in a pathological setting and that tumor vessels lacking *Lrg1* tend to be larger, raise the possibility that LRG1 affects tumor vascularization.

The observed loss of small vessels, with a concomitant increase in larger vessels, is a characteristic associated with vessel normalization¹³ and suggests that the presence of LRG1 may impair vessel maturation. Pericyte coverage and basement membrane deposition are additional features associated with vessel stabilization and maturation⁴¹, and the failure of these processes is known to contribute to vessel dysfunction⁴². We therefore investigated whether the absence of LRG1 affects this critical relationship. Using NG2 and/or α -SMA as markers of mural cells, we observed that *Lrg1* deletion in the B16-F0, *Apc*^{Min/+} and *vil*^{CreER} *Apc*^{fl/+} models was associated with increased mural cell coverage of endothelial cells (Figures 3D and 3E). While a similar trend was observed in the LLC and KPC models, this did not reach significance. Similarly, vessels from B16-F0, *Apc*^{Min/+} and *vil*^{CreER} *Apc*^{fl/+} tumors, but not those from the LLC or KPC tumors, also exhibited increased basement membrane association (Figures 3F and S2D). In further support of the observation that *Lrg1* deletion improves vascular structure, scanning electron micrographs of B16-F0 tumors from *Lrg1*^{-/-} mice revealed a reduction in the amount of intraluminal membranous inclusions (Figure 3G), a recognized feature of abnormal tumor vessels⁴³. These data indicate that not only does *Lrg1* KO affect tumor size and survival but also its loss is associated with the acquisition of a more normal vascular appearance.

LRG1 antibody blockade replicates *Lrg1* deletion and results in improved vascular function

Having demonstrated that the deletion of *Lrg1* influences tumor growth, we next asked whether this could be phenocopied by inhibiting the activity of LRG1 in WT mice with a LRG1 function-blocking antibody. B16-F0 tumor-bearing mice, which exhibited robust effects of *Lrg1* deletion and which are generally considered to respond poorly to therapeutic intervention, were treated intraperitoneally with 15C4, a LRG1 function-

blocking monoclonal antibody⁴⁴. As with *Lrg1*^{-/-} mice, LRG1 antibody blockade resulted in a similar reduction in the tumor volume of 39% at the experimental endpoint (Figures 4A and S2E). As antibody blockade of LRG1 affects primary tumor growth, we next investigated its effect on the LLC tumor metastasis model. Metastasis-bearing mice were treated perioperatively with 15C4 (Figure S1C), resulting in a significant improvement in survival (Figure 4B), showing that LRG1 antibody blockade not only replicates the therapeutic effect of *Lrg1* KO on primary tumor growth but also affects metastatic cancer.

We then assessed whether antibody blockade changes vascular function in primary B16-F0 tumors. As observed in *Lrg1* KO mice, 15C4 treatment of B16-F0 tumor bearing mice resulted in a decrease in vessel density, an increase in vessel size (Figure S2F), and an increase in mural cell association with tumor vascular endothelial cells (Figure 4C). However, the increase in basement membrane coverage was not significant (Figure S2G). These data show that the inhibition of LRG1 largely recapitulates the impact of *Lrg1* genetic deletion in B16-F0 tumors, resulting in a more physiological vascular configuration that may be associated with vessel stabilization and improved vascular function.

To test this assertion, we examined whether the inhibition of LRG1 leads to enhanced tumor vessel perfusion. Using a systemically delivered fluorescent lectin tracer to mark perfused vessels and an antibody to decorate all endothelial cells in tissue sections, we observed a significant increase in the percentage of perfused B16-F0 tumor vessels in mice treated with 15C4 (Figure 4D). Moreover, this increase in vascular patency was associated with a significant reduction in tumor hypoxia (Figure 4E). Another feature of vascular normalization is reduced vascular permeability through the stabilization of endothelial cell junctions. The adherens junction protein vascular endothelial (VE)-cadherin regulates VE cell junction integrity and its enhanced expression is associated with a reduction in vascular leakage⁴⁵. In 15C4-treated mice, we observed a significant increase in the intensity of staining for endothelial VE-cadherin (Figure 4F) that is consistent with improved barrier integrity. In addition, we noticed a reduction in tumor vessel permeability, as indicated by limited diffusion of Hoechst dye from perfused (lectin⁺) vessels (Figure 4G). Vascular normalization also resulted in a small but non-significant increase in CD3⁺ T cells (Figure 4H). These data indicate that LRG1 blockade improves vascular function, and in so doing, confirms LRG1 both as an angiopathic factor and potential therapeutic target in tumors.

To investigate whether *Lrg1* KO or LRG1 blockade alters the expression of key signaling axes genes involved in either vascular maturation or destabilization, we undertook RNA sequencing (RNA-seq) analysis of B16-F0 tumor samples from *Lrg1* KO and WT mice and from endothelial cells isolated from either 15C4 or immunoglobulin G (IgG) control treated B16-F0 tumors. Accordingly, we investigated signature genes for the receptor-ligand pathways of VEGF, angiotensin (ANGPT), platelet-derived growth factor (PDGF), TGF- β , sphingosine 1-phosphate (S1P), Notch, Wnt, Hedgehog, fibroblast growth factor, ephrin, and apelin in tumor tissue and in isolated tumor endothelial cells (Figure S3). We also investigated the expression of key glycolytic pathway genes that have been associated with angiogenesis⁴⁶ and vascular dysregulation⁴⁷. No significant differences were observed except for an increase in the KO mouse tumors of the flow-sensitive transcription factor

Kruppel-like factor 2 (*Klf2*) (Figure S3A), and in the 15C4-treated endothelium, a decrease in the type 1 transmembrane family member *Notch2* (Figure S3B).

These data suggest that the dysregulation of these genes may not be responsible for the LRG1 effects, or that LRG1 may operate post-translationally by affecting signaling mechanisms. To address the latter possibility, we investigated whether LRG1 inhibition altered the phosphorylation status of intermediate signaling components associated with the canonical and non-canonical TGF- β pathways. Using whole-tumor protein lysates, we observed that the expression of the phosphorylated kinases AKT and ERK1/2, but not of JNK or p38, was significantly reduced in 15C4-treated mice (Figure S4A). While this does not reveal the cell source or the upstream origin, it is consistent with an effect on non-Smad-mediated TGF- β signaling and demonstrates that 15C4 is affecting the tumor signaling environment. Moreover, we also observed a significant reduction in the phosphorylation of SMAD3 (Figure S4B), suggesting that in the tumor mass, 15C4 results in inhibition of the SMAD2/3 arm of canonical TGF- β signaling.

The gene expression profiles of key endothelial cell adhesion molecules were also investigated as these have been reported to be suppressed in tumor vasculature and contribute to endothelial cell anergy. We observed elevated expression of most of the common adhesion molecules, with *Icam1* and *Vcam1* being significantly increased (Figure S4C), further supporting the contention that the vasculature is normalized by *Lrg1* deletion.

Inhibition of LRG1 increases the delivery and efficacy of chemotherapy

While LRG1 may affect various aspects of tumor biology, we focused on the possibility that vascular normalization, through inhibition of LRG1, may be exploited to enhance the delivery of additional therapeutic agents. To test whether LRG1 blockade enhances the efficacy of a co-therapy, we investigated 15C4 in combination with the cytotoxic agent cisplatin in the B16-F0 subcutaneous model. While both 15C4 and the maximum tolerated regimen of cisplatin each elicited a reduction in tumor size, their delivery in combination was significantly more effective (Figures 5A and S5A). Analysis of the growth rates of individual tumors showed that the combined therapy of 15C4 and cisplatin was 25% more effective at inhibiting tumor growth than control IgG and cisplatin (Figure 5B). Consistent with this and the hypothesis that 15C4 enhances the delivery of cisplatin to the tumor, we saw a large increase in DNA double-stranded breaks, as revealed by γ -H2AX positivity (Figure 5C), and apoptosis (Figure 5D), demonstrating that inhibition of LRG1 improves the delivery, and hence, efficacy, of a cytotoxic drug.

LRG1 inhibition enhances the efficacy of adoptive cell therapy

These results led us to ask whether a similar enhancement of tumor cell killing could be achieved with other therapeutic modalities. In particular, we sought to establish whether in such a generally treatment-refractive tumor we could enhance the effect of immunotherapies. We therefore investigated the combination of LRG1 antibody blockade and adoptive T cell therapy. Following subcutaneous grafting of B16-F10 melanoma cells harboring the internal influenza nucleoprotein antigen NP68 (NP68-B16)³⁷, donor F5B6 CD8⁺ T cells expressing a T cell receptor (TCR) specific for the NP68 peptide were transferred to

the tumor-bearing host mice. As previously described⁴⁸, F5B6 CD8⁺ T cells significantly reduced tumor growth (Figures 6A and S5B). However, the combination of 15C4 with this dose of adoptive T cells led to a 30% greater reduction in tumor growth rate (Figures 6A and 6B). Upon histological analysis, the number of CD3⁺ T cells that had infiltrated the tumor increased marginally in the 15C4 alone and donor CD8⁺ T cell groups but following combination therapy was elevated significantly, predominantly as a result of donor CD8⁺ T cell (CD90.2⁺) infiltration (Figure 6C). The effects on tumor growth and T cell entry were replicated in a subsequent study in which the mice were treated with a reduced titer of F5B6 CD8⁺ T cells, but with the same dose of 15C4 antibody and extended for a further 13 days (Figures 6D and S6A). Again, an increase in tumor-infiltrating lymphocytes (TILs), particularly antigen-activated donor cells, was observed, which is consistent with vascular normalization and improved delivery. We also observed less peritumoral T cell cuffing and an associated increase in the density of intratumoral TILs (Figure S6B), suggesting that migration from the tumor vascular margin through the stroma is also enhanced in 15C4-treated tumors.

LRG1 inhibition augments the effect of PD1 checkpoint inhibition

The use of immune checkpoint antagonists, including inhibitors of CTLA-4, PD1, and PDL1, has proven to be very effective in the treatment of hematological cancers and melanoma, but their impact on many solid cancers has been less effective. Having shown that 15C4 treatment enhanced the efficacy of adoptive T cell therapy, we investigated whether 15C4 could also augment the effectiveness of a checkpoint inhibitor. B16-F0 cells were grafted into WT mice, followed by treatment with 15C4, an anti-PD1 blocking antibody, or a combination of both. As monotherapies, 15C4 and anti-PD1 each elicited a significant reduction in tumor volume (Figures 7A and S6C) and mean growth rate (Figure 7B), with anti-PD1 producing 33% tumor growth inhibition (TGI). In combination with 15C4, however, overall TGI was 88%, with evidence of tumor regression occurring at the later time point (Figure S6C). Histological analysis at the study endpoint revealed increased CD8⁺ T cell infiltration in the combination therapy group (Figures 7C and 7D). Consistent with this, we also observed enhanced granzyme B expression (Figures 7C and 7E), indicative of greater cytotoxic lymphocyte activity.

To establish whether we could replicate this effect in another tumor model, we returned to the LLC subcutaneous tumor, which has been reported to be non-responsive to checkpoint inhibition⁴⁹⁻⁵¹. Using an identical treatment strategy to that used with the B16-F0 tumors, monotherapy with anti-PD1 did not affect tumor growth, whereas 15C4 treatment, as reported above, brought about a modest but significant reduction. Combination therapy, however, resulted in a significant reduction in tumor growth compared to IgG control ($p < 0.0001$) or anti-PD1 ($p < 0.002$) alone (Figure 7A). Moreover, as observed in the B16-F0 tumors, we also recorded a change in the profile of infiltrated immune cells, in which a significant increase in CD3⁺ T cells was observed (Figures S7B and 7C). Furthermore, the extent of granzyme B activity was also significantly increased in the combination arm (Figure S7D).

Combination of anti-LRG1 and anti-PD1 does not induce the formation of HEV

It has previously been shown that the combination of vascular normalizing agents and checkpoint inhibitors can stimulate the formation of HEVs and that this may play a significant role in driving enhanced leukocyte recruitment and subsequent improved tumor cell killing⁵². To determine whether our combined therapy also induced HEV formation, we undertook qPCR analysis of a panel of HEV signature genes, namely glycosylation-dependent cell adhesion molecule 1 (*Glycam1*), and the chemokines *Ccl19*, *Ccl21*, and *Cxcl13*¹⁴. No significant differences in the expression of these genes between control and treatment arms was observed (Figure S7E), indicating that HEV induction did not contribute to the therapeutic effect. This was further confirmed by immunohistological staining of tumor sections with the MECA79 antibody, which detects peripheral node addressin (PNAd), revealing a lack of signal in control and treatment groups (Figure S7F). Similarly, in the LLC tumor, we were unable to detect MECA79 staining showing that in this model, LRG1 blockade also does not drive HEV formation (Figure S7G). These data indicate, therefore, that while HEV formation in other settings may be a contributing factor to the observed increase in TILs and treatment efficacy, it is not the only mechanism through which a combination of vascular normalizing strategies with immune checkpoint inhibition can elicit a beneficial effect.

Discussion

In this study, we provide new insight into the cause of dysfunctional vessel growth in tumors and show that LRG1 is a significant angiopathic factor capable of disrupting the normal angiogenic process and contributing to the pro-oncogenic microenvironment of primary tumors. Under normal conditions, the principal source of LRG1 is the liver, where it may serve as an acute phase protein⁵³ involved in wound healing^{54,55}. In many diseases, however, LRG1 is induced locally in tissue lesions by the vascular endothelia and, in the case of cancer, by surrounding tumor cells. Locally produced LRG1 is known to contribute to the formation of abnormal vessels in the eye and kidney^{1,2}, in part by disrupting homeostatic TGF- β signaling in a highly context-dependent manner. Here, we have shown that LRG1 also affects the vasculature of tumors and that deletion of the *Lrg1* gene, or inhibition of LRG1 function with a blocking antibody, improves vessel structure and function. Our data indicate that LRG1 is not directly pro-angiogenic, but most likely facilitates neovascularization through its destabilizing effect on pericyte-endothelial cell interactions, a prerequisite for angiogenic sprouting⁵⁶. The decrease in vessel density observed in some models, in the absence of *Lrg1* or following antibody blockade, may therefore reflect vascular stabilization and subsequent suppression of angiogenesis. These improvements in vessel function were mediated independently of any alterations in gene expression of cardinal ligand-receptor pathways involved in determining vascular status, including members of the VEGF signaling network. One gene that was found to be altered significantly was the shear response factor *Klf2*. The upregulation of *Klf2* is consistent with a shift from turbulent oscillatory flow to uniform laminar flow and is in accordance with the observed vascular normalization⁵⁷. KLF2 can be transcriptionally activated through TGF- β /ALK5 signaling⁵⁸ and is consistent with LRG1 biasing the TGF- β signaling in the endothelium in favor of the destabilizing ALK1-Smad 1/5/8 pathway^{1,2} and away from

angiostatic ALK5-Smad2/3 signaling. *Lrg1* deletion, therefore, may lead to the maintenance of TGF- β /ALK5 signaling and vascular quiescence. Contrary to this, our observation that 15C4 causes a decrease in Smad3 phosphorylation in the tumor mass suggests that it affects TGF- β signaling differently in different cells within this setting, further illustrating the highly context-dependent nature of the TGF- β signaling pathway. It has been reported that TGF- β 1 enhances antigen-induced PD1 expression through Smad 3-dependent transcriptional activation in T cells⁵⁹ and that natural killer (NK) cell differentiation and antitumor function rely on Smad3 phosphorylation⁶⁰. Its inhibition by a LRG1 blocking antibody may, therefore, contribute to an enhanced immune response and illustrates the growing evidence that LRG1 not only affects the vasculature but is also pleiotropic in its mode of action. Our observation that the Notch2 gene is downregulated in tumor endothelial cells following 15C4 treatment points to LRG1 playing a role in the Notch pathway, where it has a recognized role in promoting angiogenesis. Consistent with our finding of suppressed ERK phosphorylation, it has been shown that mitogen-activated protein kinase (MAPK) activation in cancer cells results in the induction of *Jagged1* and the activation of angiogenesis through Notch signaling⁶¹. Clearly, these possibilities would require further investigation to establish a causal link.

The decrease in tumor growth and improvement in survival with deletion or blockade of LRG1 on its own may be a consequence of decreased angiogenesis and/or due to associated effects on the TME. For example, improved oxygenation resulting from better perfusion is likely to reverse hypoxia-mediated changes such as the activation of pro-oncogenic hypoxia-inducible factor 1 (HIF1)-mediated genes, selection and expansion of aggressive clones, and immune evasion^{62–65}. A further contributing factor may be a direct effect of LRG1 on cancer cells, where it has been reported to stimulate proliferation and migration^{34,66}. These deleterious effects of LRG1 are, however, at odds with a previous report of its suppression of LLC tumor growth⁶⁷, but are consistent with overwhelming clinical evidence that increased circulating LRG1 levels are diagnostic and associated with poor prognosis^{27–39}. Our finding shows that blocking LRG1 in a metastatic model is of considerable potential therapeutic importance, particularly as metastatic spread is the primary cause of cancer mortality. In a complementary study, we have found that LRG1 primes the vasculature for metastatic seeding and that its inhibition renders metastatic sites less permissive for metastatic growth⁶⁸. Moreover, it has also been reported recently that *Lrg1* KO reduces B16F10 seeding to the lungs following intravascular tumor cell delivery⁶⁹, further corroborating LRG1 as a therapeutic target for reducing metastatic spread.

The discovery that LRG1 is angiopathic led us to test the hypothesis that blocking LRG1 would improve vascular function and augment the effects of other therapies. Treatment of tumorbearing mice with 15C4 significantly enhanced the cytotoxic effect of cisplatin, suggesting that vascular normalization permits more effective delivery of the drug to the tumor mass. The combination of 15C4 and cisplatin exhibited not only reduced growth rate but also evidence of tumor regression that was not evident with monotherapy. The increased tumor cell death may also be enhanced through improved tumor oxygenation, as hypoxia attenuates the effectiveness of cisplatin and contributes to chemotherapeutic resistance⁷⁰. Consistent with the cisplatin study, the blockade of LRG1 also improved the efficacy of adoptive T cell therapy. The B16-F0 mouse tumor model is not considered a very

immunologically active tumor and, under normal conditions, exhibits limited TILs compared to other models. This was confirmed in B16-F10 melanoma cells expressing the NP68 internal influenza nucleoprotein antigen as a surrogate tumor antigen, in which very few infiltrated CD3⁺ T cells were seen in the untreated mice. Adoptive cell therapy with NP68 antigen-specific CD8⁺ T cells led to reduced tumor growth, but this did not correlate with a significant increase in the number of infiltrated CD3⁺ T cells in end-stage tumors, as has been noted previously in this model⁷¹. This is likely to reflect the dynamic nature of T cell involvement, in which single endpoint analysis does not record possible temporal changes in T cell recruitment, retention, exit, proliferation, and death. Nevertheless, what was strikingly clear was that in the presence of LRG1 inhibition, adoptive T cell therapy led to greater tumor destruction, and a significant increase in total CD3⁺ T cells that were predominantly derived from the injected cells. This undoubtedly reflects the antigen-activated status of the donor cells and their enhanced migratory and retention capacity compared to circulating naive T cells. The improved vascular patency brought about by blocking LRG1 therefore results in better access to the tumor vascular bed, enabling greater penetration into the tumor mass⁷²⁻⁷⁴. It is also likely that improved oxygenation will counteract some of the negative effects of hypoxia that may affect T cell proliferation, retention, and survival within the TME.

As with cisplatin and adoptive T cell therapy, blocking LRG1 with 15C4 also vastly improves the efficacy of a checkpoint inhibitor, even in the highly resistant LLC model⁴⁹⁻⁵¹. It has long been recognized that tumors can evade immune rejection through eliciting powerful immunosuppressive signals that prevent an effective T cell response. This negative immunoregulation can be impeded through the use of immune checkpoint inhibitors,^{75,76} which in certain human cancers has led to marked improvements in tumor destruction and overall survival. However, many cancers remain immunologically silent for multifactorial reasons⁷⁷, but may include impaired immune cell delivery due to compromised perfusion^{73,74}. This has led to the concept that vascular normalization strategies targeting VEGF, or other vascular modulating factors such as angiopoietin 2, endothelial glycoprotein L1, notch 1, and regulator of G protein signaling 5 (Rgs5)²², may enhance effector cell entry to the tumor. These studies revealed a profound crosstalk between the vasculature and the tumor immune microenvironment. Accordingly, vascular normalization promotes the infiltration of immune cells but can also enhance the expression of immune modulators such as the checkpoint ligand PD-L1¹⁴⁻¹⁶. Consistent with this crosstalk, it has been reported that abnormalization of the vasculature decreases immune cell infiltration and that deletion of CD4⁺ T cells promotes dysfunctional vessels²⁵, revealing the close functional interplay between the immune system and the vasculature.

Improved lymphocyte infiltration previously reported with vascular normalization has been attributed to the formation of HEV⁵². These structures, normally present in lymph nodes, are characterized by a plump morphology and expression of specialized adhesion molecules, including PNA_d, that facilitate leukocyte traffic. Their induction in tumors, therefore, has provided a mechanistic explanation for the increased presence of TILs and enhanced tumor killing observed in combination therapies. In our setting, however, we were unable to observe the presence of HEV as determined by a panel of distinguishing markers. Other factors, over and above improved perfusion, may therefore be responsible for the enhanced

infiltration observed. One feature of tumor endothelial cells that may contribute to poor leukocyte recruitment is their failure to respond effectively to activation by inflammatory mediators, a condition called endothelial cell anergy⁷⁸. This manifests in part as a loss of expression of key cell adhesion molecules, such as intercellular adhesion molecule 1 (ICAM-1) and vascular cell adhesion molecule 1 (VCAM-1)^{79,80}, which are required for effective leukocyte recruitment⁸¹. Here, we show that vascular normalization, brought about by *Lrg1* deletion, reverses in part this anergy by enhancing the induction of *Icam1* and *Vcam1*, which in turn, will facilitate the recruitment of circulating leukocytes⁸². This demonstrates that in addition to HEV formation, other mechanisms brought about by vascular normalization are at play in facilitating leukocyte tumor infiltration.

Our finding that inhibiting LRG1 with a function-blocking antibody reverses its detrimental effects on the tumor vasculature and enhances both adoptive T cell and immune checkpoint inhibition strategies lends further weight to the view that improving vascular function is a promising co-therapeutic strategy. Targeting LRG1, therefore, may provide an additional, or alternative, approach for normalizing the tumor vasculature and enhancing the efficacy of cotherapies. At present, the principal approach is to use anti-VEGF axis inhibitors, which have shown some capacity to normalize the vasculature and improve immunotherapies¹⁴. However, major challenges with this approach remain, not the least of which is the difficulty in determining the appropriate dose and the purported short therapeutic window^{6,9}. This is confounded by difficulties in determining the relative activity of the VEGF axis in different tumors¹³. Unlike VEGF-targeted therapies, blocking LRG1 has the potential advantage that patients may be stratified, as higher circulating levels generally correlate with a worse 27–39 prognosis^{27–39}.

As interest in vascular normalization increases, various targets, other than those of the VEGF axis, have been identified²², but for most, their clinical utility remains untested. Here, we present LRG1 as a promising target, but its safety and successful translation into patients need to be proven. Unlike some targets, however, *Lrg1* KO in the mouse does not produce an overt phenotype and they remain fertile and healthy over a normal lifespan, providing evidence that it is not critical to homeostasis. In addition, as an ectopic non-essential modifier of TGF- β signaling, LRG1 blockade may offer advantages over direct therapeutic targeting of the TGF- β superfamily for treating cancer, which in general has been disappointing. Failure in this area is likely due to the difficulty in separating homeostatic from pathogenic TGF- β signaling as many core TGF- β signaling components are involved in both. TGF- β operates as an analog signaling network whose effects are largely determined by a balance of complex and nuanced interactions between different arms of the extensive signaling cascade. Under normal conditions, homeostatic TGF- β signaling is required for a stable vasculature, but during disease this is disturbed, and LRG1 is a prime disrupting candidate. However, targeting the LRG1 binding partner endoglin (ENG), which is upregulated on neovascular endothelia, has proven to be disappointing in achieving a therapeutic effect on tumor angiogenesis, although any impact on vascular normalization has not been fully investigated. This failure may be due, in part, to antagonizing a binding site important for maintaining vascular quiescence⁸³. Interestingly, LRG1 binding to ENG facilitates the reconfiguration of the TGF- β receptor complex to enhance pathogenic signaling, but in so doing, may also result in the loss of beneficial homeostatic BMP9/ENG

signaling. Targeting LRG1, therefore, removes an independent pathogenic factor that disturbs the homeostatic balance in TGF- β signaling without interfering with essential components of the network.

In conclusion, we have shown that LRG1 is a major driver of abnormal vessel growth in solid primary tumors and that its inhibition leads to significant restoration of normal vascular function. This raises the possibility that therapeutic targeting of LRG1 will improve the quality of vessels not only in cancer but also in diseases as diverse as diabetic kidney disease, neovascular age-related macular degeneration, and inflammatory disease, and pave the way toward improved strategies to revascularize ischemic tissue.

Limitations of Study

While there is growing evidence that LRG1 is playing a role in human cancer, and experimental animal work indicates its utility as a therapeutic target, the translatability of this approach to humans remains unproven. Work using subcutaneous tumor models in combination therapy will ideally need further corroboration in models that are considered more representative of human cancer. In particular, patient derived xenograph models may provide additional evidence of efficacy, although such models are complex and challenging when investigating the effect of immunotherapies. Nevertheless, despite these limitations the finding that LRG1 plays a role in genetically engineered mouse models and in a metastasis model provides confidence that this may be successfully translated into patients.

Experimental Model And Subject Details

Human samples

Fresh frozen normal lung and lung squamous cell carcinoma tissue were obtained from Proteogenex Inc (<https://www.proteogenex.com>). Formalin-fixed paraffin-embedded prostate cancer tissue was obtained from Amsbio (<https://www.amsbio.com>) and normal human breast and ductal breast carcinoma from Pantomics Inc (<https://www.pantomics.com>). Human serum samples from normal healthy subjects and from treatment naïve cancer patients with colorectal adenocarcinoma, pancreatic adenocarcinoma and squamous cell lung carcinoma, were obtained from Proteogenex, Inc.

All specimens from commercial sources were collected under ethical regulations and in accordance with all applicable (local and international) laws. Commercial clinical materials were obtained following official protocols, with appropriate Institutional Review Board/Independent Ethics Committee (IRB/IEC) approval operating in accordance with Federal Regulations in addition to ICH, HIPAA, and GCP guidelines pertaining to the protection of human subjects. All donors or their relatives voluntarily signed legal Informed Consent documents and specimens were de-identified and de-linked from the original clinical records.

Mice

All procedures in the UK were performed in accordance with the UK Animals (Scientific Procedures) Act and the Animal Welfare and the Ethical Review Bodies of the UCL Institute

of Ophthalmology, Cancer Research UK Beatson Institute, University of Glasgow, and Cardiff University. All procedures in Germany were approved by governmental (G164/16, G231/16, G254/18, G286/18, G9/19, G196/19, and G213/18 from Regierungspräsidium Karlsruhe, Germany) and Institutional (IRCBC-2018-006 to J.H.) Animal Care and Use Committees. All experiments were performed in accordance with the respective institutional guidelines for the care and use of laboratory animals. All mice were housed in specific pathogen-free animal facilities had a 12-hour light/12-hour dark cycle with free access to food and drinking water. Where possible, preliminary experiments were undertaken to establish sample sizes, whilst addressing ethical and reductionist animal use considerations.

For subcutaneous graft models male C57BL/6J mice of 7-8 weeks of age were purchased from Harlan Laboratories or Charles River Laboratories. *Lrg1^{-/-}* mice were generated by the University of California Davies knockout mouse project (KOMP) repository (<http://www.komp.org/>) and bred in-house. Genetically engineered male and female mice were bred and housed in the animal facility at the CRUK Beatson Institute. All experiments on genetically engineered mouse models were performed on a C57BL/6 background. For the metastatic model C57BL/6N mice were purchased from Charles River Laboratories and used between 8 and 12 weeks of age. All mice were housed in the DKFZ animal facility on a 12-hour light/12-hour dark cycle with free access to food and drinking water in specific pathogen-free animal facilities.

Method Details

Cell Culture

Mouse cancer cell lines B16-F0 (mouse melanoma cell line), NP68-B16 (mouse melanoma B16F10 cells expressing NP68 peptide and LLC1 (LL/2; mouse Lewis Lung carcinoma) were maintained in Dulbecco's Modified Eagle's Medium supplemented with glucose (4.5 g/L), sodium pyruvate (110 mg/L), 10% FBS, penicillin (100,000 U/L) and streptomycin sulphate (100 mg/L) at 37°C in 5% CO₂ and checked to be clear of mycoplasma contamination.

Tumor models

For subcutaneous tumors single-cell suspensions of 1×10^6 B16-F0 or LLC cells were injected subcutaneously into a single dorsal flank of *Lrg1^{+/+}* or *Lrg1^{-/-}* 8-16 week old male C57BL/6J mice in 100 μ l PBS. Mice were randomized by age prior to inoculation. Tumors were measured by evaluators, blinded to treatment, at defined intervals using calipers and tumor volume was calculated using the formula: $V = (4/3) \times \pi \times (L/2) \times (W/2) \times (H/2)$. Mice were sacrificed at the end of the experiment, or when tumors reached the permitted humane endpoint. The mean tumor growth rate for individual tumors was calculated using the slope of log transformed tumor volumes⁷¹.

For ageing experiments in the *Apc^{Min/+}* and KPC genetically engineered spontaneous mouse tumor models^{84,85}, mice were sampled when showing moderate signs of illness. Tumors in *villin^{CreER} Apc^{fl/+}* mice^{86,87} were induced at an age of 6-10 weeks by a single intra peritoneal injection of 2 mg Tamoxifen in corn oil, and aged until showing moderate

signs of illness. No distinction between males and females was made in any of the mouse experiments and researchers were blinded for Lrg1 status.

In the metastatic model LLC tumors were allowed to develop following subcutaneous inoculation of 1×10^6 LLC cells in PBS in C57BL/6N mice. Primary tumours were surgically resected at an average size of 300 mm^3 . Perioperative treatment was initiated once the primary tumour size reached an average of 150 mm^3 and continued until 10 days following primary tumour resection. Tumors were resected at an average size of 300 mm^3 . Mice were administered with either anti-LRG1 (15C4) or control IgG (50 mg/kg) twice a week and routinely checked for the experimental endpoint criteria. Mice were randomly assigned by a blinded scientist into the cohorts of treatment at the time of therapy initiation. For the RNAscope analysis of metastases-bearing lung tissue, samples were collected approximately three weeks post-primary tumor resection.

ELISA

96 well Maxi-Sorp immunoplates (Fisher 10547781) were coated with $40 \mu\text{g/ml}$ 15C4 ($50 \mu\text{l/well}$) in $0.2\text{M NaCO}_3/\text{NaHCO}_3$ buffer pH9.4 and incubated overnight at 4°C . The plates were washed 3 times with 0.1% Tween-20/PBS, blocked with 3% BSA/PBS for 1h at RT and washed again 3 times. Patient samples and LRG1 standards (range 0 - 6000ng/ml) were diluted with 0.1% Tween-20/PBS and left to incubate overnight at 4°C . Plates were washed 3 times before adding anti-LRG1 pAb (Atlas Antibodies) in PBS and incubated for 1.5h at room temperature. Plates were washed 3 times before adding HRP goat anti-rabbit (Dako) in PBS for 1.5h at room temperature. The plates were washed 3 times and ELISA substrate reagent kit (R&D Systems) was used at 1:1 ratio and left to develop in the dark. 2N sulphuric acid was used to stop the reaction and plates were read at 450nm (reference wavelength 540nm).

Immunohistochemistry

Human tumor sections: For human lung tissue, cryosections were cut at a nominal $5 \mu\text{m}$ thickness, washed, blocked with milk powder and stained with humanized 15C4 (Magacizumab) or natural human IgG4 (Abcam) that were FITC conjugated using the commercial FluoroTag conjugation kit (Sigma-Aldrich). Following washing and blocking with milk powder, primary antibodies were incubated for 1h at room temperature at a concentration of $0.078 \mu\text{g/ml}$. Sections were washed and treated with Dako Envision⁺ system HRP labeled polymer anti-rabbit for 30min. After further washing sections were treated with Liquid DAB+ substrate chromogen system for 10min and 0.5% copper sulphate solution for 5min followed by counterstaining with haematoxylin for 1min.

Formalin-fixed paraffin-embedded sections of prostate or breast tissue were cut at $5 \mu\text{m}$ thickness and treated with either anti-LRG1 rabbit polyclonal antibody (Proteintech) at 1:200 dilution or anti LRG1 monoclonal antibody 15C4 at $10 \mu\text{g/ml}$. Following antigen heat retrieval with a Leica ER2, sections were processed on the Leica Bond III platform.

Paraffin embedded mouse tumor sections: the small intestine and colon from *Apc^{Min/+}* and the *vil^{CreER} Apc^{fl/+}* tumors were formalin-fixed and paraffin-embedded (FFPE). $5 \mu\text{m}$ sections were deparaffinized and immunolabelled following antigen retrieval before being

fixed in 4% paraformaldehyde, 100% methanol or 100% acetone, depending on antibodies used. Sections were blocked in 0.5% BSA and washed in 0.01% Tween-20 in PBS.

Fresh frozen mouse tumor sections: subcutaneous B16-F0, LLC, KPC and PDAC tumours were fresh frozen on dry-ice and embedded in optimal-cutting-temperature medium (OCT). Contiguous frozen tissue sections were cut at a thickness of 8 μm or 20 μm and stored at -20°C . Sections were fixed immediately in 4% paraformaldehyde, 100% methanol or 100% acetone, washed in PBS, permeabilized in 0.1% Tween-20 in PBS for 10min, washed again in PBS and blocked in 1% BSA for 1h at room temperature. Primary antibodies were incubated overnight at 4°C in 0.5% BSA with or without 0.01% Triton-X100 in PBS. The antibodies used to label mouse endothelium were anti-CD31 (Dianova or Abcam), endomucin (Abcam), anti-VE-cadherin (Santa Cruz) and anti-podocalyxin (PDXL; R&D systems), with the latter used in B16-F0 tumours as it strongly labelled the endothelium and the staining pattern was almost indistinguishable from CD31 in this model (data not shown). Mural cells were labeled with antibodies to NG2 (Merck-Millipore) or αSMA (Sigma-Aldrich). Antibodies to basement membrane proteins collagen-IV (Merck-Millipore) or perlecan (Abcam), and immune cell markers CD3 (Abcam), CD8 (Novus), or CD90.2 (Biolegend) were also used. Other primary antibodies were to granzymeB (Novus) and EF5 (Merck-Millipore). Alexa-fluor labeled secondary antibodies (ThermoFisher) were incubated in 0.5% BSA with or without 0.01% Triton X100 at room temperature for 1h. Both primary and secondary antibodies were washed three times for 15 min, either in 0.01% Tween-20 in PBS or PBS only, depending on the antibody. The slides were mounted using anti-fade mounting medium (ProLong Gold or Dako). For the CD8 and granzymeB co-staining protocol, samples were processed as described above except that they were fixed in 2% PFA in PBS, dropped in PBS, fixed again for 3min in methanol at -20°C , washed in distilled water and 0.01% Tween-20 in PBS for 5min. The antibodies (1:100) were incubated in 0.5% BSA with 0.001% Triton X100 in PBS.

RNAScope[®] in situ hybridisation

FFPE tumor or intestine samples were placed in xylene followed by absolute ethanol. For chromogenic detection, slides were processed using the 2.0 HD Detection kit – BROWN (Advanced Cell Diagnostics) and the manufacturer's instructions. For fluorescence detection, slides were processed using the Multiplex Fluorescent Kit v2, followed by TSA[®] signal amplification (PerkinElmer) and immunohistochemistry performed afterwards if desired. Slides were hybridized with probes specific to *Lrg1* and the quality of signal and tissue were determined using positive (Ppib) and negative (*Dapb*) probes, supplied by the manufacturer (Advanced Cell Diagnostics). The specificity of the *Lrg1* probe was confirmed by probing tumor sections from *Lrg1^{+/+}* and *Lrg1^{-/-}* mice.

Analysis of vessel density and normalisation

To measure vessel profiles in the tumors, sections were labeled with antibodies to endothelium markers (CD31, podocalyxin (PDXL) or endomucin). B16F0 and LLC sections were imaged using a Nikon Eclipse Ti epifluorescence microscope (Nikon). The entire tumor vasculature was included in the analysis, excluding vasculature in the tumor margin. KPC sections were imaged on a Zeiss 700 confocal microscope. At least two $850 \times 850 \mu\text{m}$

areas per section containing tumor vessels were imaged and maximum intensity projections of z-stacks analyzed. Vessel density (number per unit area) and size (cross-sectional area) were calculated from thresholded images from B16-F0, LLC and KPC tumors using NIS-Elements software (Nikon). Vessels were identified as individual objects between 5-800 μm^2 that were positive for the endothelial marker. The mean vessel size and density per tumor section is reported. For *Apc*^{Min/+} and the *vil*^{CreER} *Apc*^{fl/+} sections, at least 2 intestinal adenomas per mouse were imaged, using a Zeiss 700 confocal microscope and the mean result reported. Vessels in a 250x188 μm ROI at the luminal edge of the adenoma were analyzed. Since vessels were mostly contiguous in these images, vessel area per image was calculated using ImageJ, rather than vessel size and density of individual vessels.

The association of mural cells or basement membrane proteins with the tumor endothelium was measured from sections labelled with antibodies to endothelial cells (CD31, endomucin or podocalyxin) and multiple mural cell (NG2 and/or α SMA) or matrix (perlecan and collagen IV) markers. For mural cells, a 0.37 or 0.72 cm^2 ROI encompassing the edge and core of the tumor was imaged and then analyzed using NIS elements software (Nikon) or ImageJ (<http://imagej.nih.gov/ij/>). For analysis of endothelial basement membrane, at least 2 640x640 μm areas per section containing tumor vessels were imaged on a Zeiss 710 microscope and maximum intensity projections of z-stacks analyzed. The fraction of perlecan or collagen IV pixels which overlap CD31 positive pixels was calculated from a single plane through the center of the z-stack. The same threshold was used for each image and Manders' overlap coefficient was calculated using JACoP plugin on ImageJ. Data were normalized to the mean control value for each experiment. In all cases images were anonymized with respect to experimental condition before analysis.

Tumor hypoxia and vascular perfusion

To measure tumor hypoxia, 0.2 ml of 10mM EF5 (Merck-Millipore) was injected into the peritoneum of tumor bearing mice and tumors harvested after 1h. Pimonidazole adducts in sections were detected by immunohistochemistry using anti-EF5, clone ELK3-51 Cyanine 3 conjugate and the entire tumor section imaged using a Nikon Eclipse Ti epifluorescence microscope. The proportion of each tumor positive for hypoxia stain was measured from identically thresholded images on NIS elements software (Nikon) and reported as a percentage of total image area.

To examine tumor vessel perfusion and leakage, tumor-bearing mice were injected intravenously with FITC-labelled Lycopersicon esculentum lectin (Vector labs; 10 mg/kg) and low molecular weight fluorescent DNA binding dye Hoechst 33342 (Sigma-Aldrich; 7.5 mg/kg), respectively, followed 3min later by perfusion fixation with 4% paraformaldehyde. Cryosections were labelled with an antibody to endomucin to count endothelialized vessels. The percentage of perfused vessels was calculated as the % of endomucin⁺ vessels which were also lectin⁺. The proportion of each ROI positive for Hoechst was measured from thresholded images on NIS elements software (Nikon), and normalized to lectin area, i.e. perfused vessels.

Tumor co-therapy strategies

Chemotherapy—To investigate the effects of LRG1 blockade on efficacy of tumor chemotherapy, wild-type C57BL/6 mice were injected with B16-F0 cells subcutaneously into the dorsal flank and treated with 50 mg/kg of the function-blocking anti-LRG1 monoclonal antibody 15C4 or IgG control administered by intraperitoneal injection every 3 days from day 3. At day 7 and every other day thereafter, a maximum tolerated dose (2.5 mg/kg) of the chemotherapy drug cisplatin was administered by intraperitoneal injection until the mice were sacrificed at the end of the experiment or when tumors exceeded 1000 mm³. Cisplatin-induced DNA damage was assayed using an antibody against the DNA double strand break marker γ -H2AX (Merck-Millipore) on tumor sections co-stained with DAPI to enumerate cell nuclei. The percentage of nuclei with γ -H2AX foci was measured from confocal images (Zeiss 700) and analyzed by evaluators who were blinded to the experimental arm. Apoptotic cells were identified by TUNEL assays on sections using an ApopTag in situ apoptosis detection kit (Merck-Millipore).

Adoptive T cell therapy—To investigate the effects of LRG1 blockade on the efficacy of tumor immunotherapy a mouse model of adoptive T cell therapy was used as described⁴⁸. Briefly, 5×10^5 NP68-B16 melanoma cells in 200 μ l sterile PBS were injected subcutaneously into the shaven left dorsal flank of B6.PL-Thy1a/CyJ (Thy1.1/CD90.1) or C57BL/6 (Thy1.2/CD90.2) mice, tumors were grown for 6 days and the mice sub-lethally irradiated with 597cGy total body irradiation. On day 7, F5B6 CD8⁺ T cells (> 95% naive (CD62L⁺, CD44 low) CD8⁺ T cells) expressing the F5 T cell receptor for NP68 peptide on a C57BL/6 background were isolated from spleens of naïve F5B6 mice using a CD8a⁺ T cell isolation kit for negative selection, and LS columns, according to the manufacturer's instructions (StemCell Technologies). Briefly, spleens were harvested from adult mice and mashed through a 70 μ m cell strainer (BD Pharmingen). Red blood cells were lysed using red cell lysis buffer (Biolegend) and lymphocytes washed with ice-cold phosphate buffered saline (PBS) supplemented with 2% fetal calf serum (FCS) prior to magnetic isolation. The enriched CD8⁺ cell fraction was counted using a hemocytometer, resuspended in sterile PBS for injection and analyzed for CD8, CD62L, CD44, CD27 and F5 TCR expression. Tumor-bearing mice were randomly distributed into 5 treatment groups of 8-11 mice (No transfer; IgG; 15C4: IgG + F5B6; 15C4 + F5B6) and injected subcutaneously with peptide vaccine (100 μ g NP68 peptide in 200 μ l incomplete Freund's adjuvant) into the right flank prior followed by 2.25×10^5 F5B6 CD8⁺ T cells (CD90.2) injected into the tail vein. Mice were treated with 50 mg/kg of the function-blocking anti-LRG1 mouse monoclonal antibody 15C4 or IgG control administered by intraperitoneal injection commencing on the same day as T cell transfers and antibody administration was repeated every 3 days until the end of the study. Tumors were measured with calipers as described above. At the end of the experiment, mice were sacrificed and tumors were frozen on dry-ice in optimal-cutting-temperature medium (OCT) and stored at -80°C before immunostaining for either total T cells (CD3⁺) or for donor T cells (CD90.2 in tumors grown in CD90.1 mice).

Immune checkpoint blockade—To investigate the effects of LRG1 blockade on the efficacy of PD1/PDL1 axis blockade in an immunologically resistant tumor, wild-type C57BL/6J male mice 8-10 weeks of age were injected with 1×10^6 B16-F0 cells

subcutaneously into the flank. Mice were treated with a combination of 50 mg/kg of the function-blocking anti-LRG1 antibody 15C4, 200 µg rat anti-mouse PD1 (Bio X Cell) or 200 µg rat IgG2a isotype control (Bio X Cell). Mice were dosed by intraperitoneal injection commencing on day 3 and antibody administration was repeated every 3 days until the end of the study. Tumors were measured with calipers at defined intervals and tumor volumes were calculated. At the end of the experiment, mice were sacrificed and tumors were fresh frozen on dry-ice in OCT and stored at -80°C before immunostaining.

T-cell infiltration analysis

Fresh-frozen sections were fixed in 100% ice-cold methanol and/or 4% formaldehyde and labeled using antibodies to total T cells ($\text{CD}3^{+}$), donor T-cells ($\text{CD}90.2^{+}$), cytotoxic T cells ($\text{CD}8^{+}$) and/or granzyme B. For each section a $2920 \times 2920 \mu\text{m}$ or $4250 \times 4250 \mu\text{m}$ tile scan was acquired encompassing the edge and core of the tumor, using a Zeiss 710 confocal microscope. Alternatively, whole sections were imaged using the EVOS Imaging System. Maximum intensity projections of z-stacks were analyzed using NIS elements software (Nikon). Positive cells were identified by thresholding either as objects/area or as fraction of total image area.

Scanning Electron Microscopy

14 days after subcutaneous B16F0 injection, *Lrg1*^{+/+} and *Lrg1*^{-/-} mice bearing tumors were perfusion-fixed with Karnovsky fixative (2% paraformaldehyde, 2.5% glutaraldehyde), followed by immersion fixation in fixative overnight at 4°C . Vibratome sections ($200 \mu\text{m}$) were washed in PBS and then osmicated with 1% osmium tetroxide in ddH₂O for 1h. They were then washed in ddH₂O and dehydrated in alcohol. The tumor sections were then immersed in dry methanol and in hexamethyldisilazane (reagent grade >99%, Aldrich chemicals) and allowed to dry. The specimens were fixed onto aluminum stubs using a conductive carbon disc and silver paint (Agar) and were then coated with 2 nm platinum in a Cressington sputter coater. Imaging was done on a Zeiss Sigma VP SEM using the in lens detector.

RNASeq and RT-qPCR

RNA from *Lrg1*^{+/+} and *Lrg1*^{-/-} B16F0 tumors was extracted using the RNeasy mini kit (Qiagen) and analyzed for quality using the 4200 TapeStation (Agilent). mRNA was prepared from total RNA for sequencing using the Kapa riboerase library preparation kit (Agilent) and was sequenced for differential expression analysis (0.5 High output NextSeq run, 43bp paired end reads). Deseq2 method was used in R to identify differentially expressed transcripts Raw RNA sequence data have been deposited with NCBI Sequence Read Archive accession number PRJNA552723 (<https://www.ncbi.nlm.nih.gov/sra/PRJNA552723>).

Endothelial cells were isolated from the CD45-negative fraction of 15C4 or IgG control treated B16F0 tumors by cell sorting with a FITC-labelled anti-CD31 antibody. The FACS-sorted cell population was isolated in RLT RNA extraction buffer (Qiagen) and RNA quality was analysed using the 4200 TapeStation (Agilent). First strand cDNA synthesis was followed by PCR-amplification, and amplified cDNA was purified using

beads and the cDNA libraries were made using the Nextera XT kit. Sequencing was performed on an Illumina NextSeq 500 with a 75bp single read and 8bp Unique Molecular Identifier. Sequencing reads were generated for each sample before aligning to the mouse genome. Differential expression and clustering were performed from the count data using the BioConductor packages SARTools and DESeq2. Processed count files and metadata have been deposited at NCBI Gene Expression Omnibus with accession number GSE184816(<https://www.ncbi.nlm.nih.gov/geo/query/acc.cgi?acc=GSE184816>).

For RT-qPCR analysis, total RNA was isolated from B16-F0 tumors that were treated with 15C4 or irrelevant IgG as indicated in the experimental conditions. cDNA was synthesized using the LunaScript RT SuperMix Kit (New England Biolabs E3010) and gene expression was analyzed by RT-qPCR on QuantStudio 6 (Applied Biosciences) using the Luna Universal qPCR kit (New England Biolabs, M3003). Relative expression was normalized to *Actb* and *Gapdh* housekeeping genes and was determined using the Ct method. Primer sequences for the mouse genes were as follows: *Ccl19*, Forward: CAGTCACTCCCCTGTGAACC, Reverse: CAGAGTTGGGGCTGGGAAG, *Ccl21a*, Forward: AAGGCAGTGATGGAGGGGGT, Reverse: CTTAGAGTGCTTCCGGGGTG, *Cxcl13*, Forward: CAGGCCACGGTATTCTGGA, Reverse: CAGGGGGCGTAACTTGAATC, *Glycam1*, Forward: TCAGCTGCAACCACCTCAG, Reverse: TTCGTGATACGACTGGCACC.

Tissue lysate preparation and Western blotting

Frozen tumor samples (~10mg per sample) were lysed in 300 µl RIPA buffer supplemented with protease and phosphatase inhibitors. The lysates were homogenized using a pestle and mortar, followed by 30min incubation on ice with vortexing every 5min. The lysates were then centrifuged at maximum speed (21,000 x g) for 20min at 4°C, and protein concentration was estimated using a BCA colorimetric protein assay (Pierce). Lysates were subjected to SDS-PAGE and Western blotting. Specific antibodies (Cell Signalling) against p-Akt, total-Akt, p-Erk1/2, total-Erk1/2, p-SapK/Jnk, total-SapK/Jnk, p-p38, total-p38, p-Smad3 and total-Smad2/3 were used. GAPDH served as a housekeeping gene. Densitometry analysis was performed using ImageJ software.

Quantification and Statistical Analysis

All analyses were blinded. Statistical analysis was performed using Graphpad Prism version 5.0 or 7.0 for Windows (GraphPad Software, La Jolla California USA, www.graphpad.com). Definition of centre, exact n, error bars and statistical tests used for each experiment are indicated in the figure legends. All error bars show 95% confidence interval (CI) unless otherwise stated. All t tests were two-tailed. Bonferonni corrections were applied for multiple comparisons using ANOVA, unless otherwise stated. A P value less than 0.05 was considered statistically significant. Grubb's test was used to test for outliers (www.graphpad.com), which were removed before analysis. For in vivo studies, group sizes were determined using historical data to reach a statistical power of at least 80% for the relevant effect size (<http://powerandsamplesize.com>). For all figures p values are represented as follows: *p < 0.05; **p < 0.01; ***p < 0.001, ****p < 0.0001.

Supplementary Material

Refer to Web version on PubMed Central for supplementary material.

Acknowledgments

J.G. and S.E.M. would like to thank Dr. Vineeta Tripathi for her work on the development of the 15C4 antibody. We would like to thank the Biological Resources Unit at the UCL Institute of Ophthalmology and the Joint Biological Services at Cardiff University. We also thank Core Services and Advanced Technologies at the Cancer Research UK Beatson Institute (C596/A17196), with particular thanks to the Biological Services Unit and Histology. This work was supported by funding to J.G. and S.E.M. from the Wellcome Trust Investigator Award 206413/B/17/Z (L.D., C.P., C.C., and A.D.); the Medical Research Council UK project grant G1000466, DPFS/DCS award MR/N006410/1 (X.W., J. George, and D.M.K.); the Confidence in Concept award MC/PC/14118 (D.M.K.); the British Heart Foundation project grant PG/16/50/32182 (M.N.O. and A.D.); Rosetrees Trust; UCL POC fund; and the UCL Technology Fund (C.C., C.P., and C.E.B.). J.G. and S.E.M. were also supported by the National Institute for Health Research (NIHR) Biomedical Research Centre based at Moorfields Eye Hospital NHS Foundation Trust and UCL Institute of Ophthalmology. The views expressed are those of the author(s) and not necessarily those of the NHS, the NIHR, or the Department of Health. A.A. received funding from Medical Research Council UK grant MR/L008742/1 (H.A.W.), Health and Care Research Wales grant CA05 (M.A. and J.O.), and Cancer Research UK grant C42412/A24416. O.J.S. was supported by an ERC Starter grant (ColonCan 311301) and by core funding from CRUK awarded to the CRUK Beatson Institute (A17196). The work by H.G.A. and M.S. was supported by grants from the Deutsche Forschungsgemeinschaft (DFG) (project C5 within CRC1366 “Vascular control of organ function” [project no. 39404578, H.G.A.] and the European Research Council Advanced Grant “AngioMature” (project 787181, H.G.A.). The graphical abstract was created with BioRender.com.

References

1. Wang X, Abraham S, McKenzie JA, Jeffs N, Swire M, Tripathi VB, Luhmann UF, Lange CA, Zhai Z, Arthur HM, Bainbridge JW, et al. LRG1 promotes angiogenesis by modulating endothelial TGF- β signalling. *Nature*. 2013; 499: 306–311. [PubMed: 23868260]
2. Hong Q, Zhang L, Fu J, Verghese DA, Chauhan K, Nadkarni GN, Li Z, Ju W, Kretzler M, Cai GY, Chen XM, et al. LRG1 promotes diabetic kidney disease progression by enhancing TGF- β -induced angiogenesis. *J Am Soc Nephrol*. 2019; 30: 546–562. [PubMed: 30858225]
3. Folkman J. Tumor angiogenesis: therapeutic implications. *N Engl J Med*. 1971; 285: 1182–1186. [PubMed: 4938153]
4. Hanahan D, Weinberg RA. Hallmarks of cancer: the next generation. *Cell*. 2011; 144: 646–674. [PubMed: 21376230]
5. Carmeliet P, Jain RK. Principles and mechanisms of vessel normalization for cancer and other angiogenic diseases. *Nat Rev Drug Discov*. 2011; 10: 417–427. [PubMed: 21629292]
6. Wong PP, Bodrug N, Hodivala-Dilke KM. Exploring novel methods for modulating tumor blood vessels in cancer treatment. *Curr Biol*. 2016; 26: R1161–R1166. [PubMed: 27825457]
7. Le Serve AW, Hellmann K. Metastases and the normalization of tumour blood vessels by ICRF 159: a new type of drug action. *Br Med J*. 1972; 4: 597–601.
8. Jain RK. Normalizing tumor vasculature with anti-angiogenic therapy: a new paradigm for combination therapy. *Nat Med*. 2001; 7: 987–989. [PubMed: 11533692]
9. Fukumura D, Kloepper J, Amoozgar Z, Duda DG, Jain RK. Enhancing cancer immunotherapy using antiangiogenics: opportunities and challenges. *Nat Rev Clin Oncol*. 2018; 15: 325–340. [PubMed: 29508855]
10. Huang Y, Yuan J, Righi E, Kamoun WS, Ancukiewicz M, Nezivar J, Santosuosso M, Martin JD, Martin MR, Vianello F, Leblanc P, et al. Vascular normalizing doses of antiangiogenic treatment reprogram the immunosuppressive tumor microenvironment and enhance immunotherapy. *Proc Natl Acad Sci USA*. 2012; 109: 17561–17566. [PubMed: 23045683]
11. Coutelle O, Schiffmann LM, Liwschitz M, Brunold M, Goede V, Hallek M, Kashkar H, Hacker UT. Dual targeting of Angiopoetin-2 and VEGF potentiates effective vascular normalisation without inducing empty basement membrane sleeves in xenograft tumours. *Br J Cancer*. 2015; 112: 495–503. [PubMed: 25562438]

12. Winkler F, Kozin SV, Tong RT, Chae SS, Booth MF, Garkavtsev I, Xu L, Hicklin DJ, Fukumura D, di Tomaso E, Munn LL, et al. Kinetics of vascular normalization by VEGFR2 blockade governs brain tumor response to radiation: role of oxygenation, angiopoietin-1, and matrix metalloproteinases. *Cancer Cell*. 2004; 6: 553–563. [PubMed: 15607960]
13. El Alaoui-Lasmali K, Faivre B. Antiangiogenic therapy: Markers of response, “normalization” and resistance. *Crit Rev Oncol Hematol*. 2018; 128: 118–129. [PubMed: 29958627]
14. Allen E, Jabouille A, Rivera LB, Lodewijckx I, Missiaen R, Steri V, Feyen K, Tawney J, Hanahan D, Michael IP, Bergers G. Combined antiangiogenic and anti-PD-L1 therapy stimulates tumor immunity through HEV formation. *Sci Transl Med*. 2017; 9 eaak9679 [PubMed: 28404866]
15. Schmittnaegel M, Rigamonti N, Kadioglu E, Cassarà A, Wyser Rmili C, Kiiialainen A, Kienast Y, Mueller HJ, Ooi CH, Laoui D, De Palma M. Dual angiopoietin-2 and VEGFA inhibition elicits antitumor immunity that is enhanced by PD-1 checkpoint blockade. *Sci Transl Med*. 2017; 9 eaak9670 [PubMed: 28404865]
16. Johansson-Percival A, He B, Li ZJ, Kjellén A, Russell K, Li J, Larma I, Ganss R. De novo induction of intratumoral lymphoid structures and vessel normalization enhances immunotherapy in resistant tumors. *Nat Immunol*. 2017; 18: 1207–1217. [PubMed: 28892469]
17. Maes H, Kuchnio A, Peric A, Moens S, Nys K, De Bock K, Quaegebeur A, Schoors S, Georgiadou M, Wouters J, Vinckier S, et al. Tumor vessel normalization by chloroquine independent of autophagy. *Cancer Cell*. 2014; 26: 190–206. [PubMed: 25117709]
18. La Porta S, Roth L, Singhal M, Mogler C, Spegg C, Schieb B, Qu X, Adams RH, Baldwin HS, Savant S, Augustin HG. Endothelial Tie1-mediated angiogenesis and vascular abnormalization promote tumor progression and metastasis. *J Clin Invest*. 2018; 128: 834–845. [PubMed: 29355844]
19. Munn LL, Jain RK. Vascular regulation of antitumor immunity. *Science*. 2019; 365: 544–545. [PubMed: 31395771]
20. Viallard C, Larrivé B. Tumor angiogenesis and vascular normalization: alternative therapeutic targets. *Angiogenesis*. 2017; 20: 409–426. [PubMed: 28660302]
21. Khan KA, Kerbel RS. Improving immunotherapy outcomes with anti-angiogenic treatments and vice versa. *Nat Rev Clin Oncol*. 2018; 15: 310–324. [PubMed: 29434333]
22. Martin JD, Seano G, Jain RK. Normalizing function of tumor vessels: Progress, opportunities, and challenges. *Annu Rev Physiol*. 2019; 81: 505–534. [PubMed: 30742782]
23. Huang Y, Kim BYS, Chan CK, Hahn SM, Weissman IL, Jiang W. Improving immune-vascular crosstalk for cancer immunotherapy. *Nat Rev Immunol*. 2018; 18: 195–203. [PubMed: 29332937]
24. Schmittnaegel M, De Palma M. Reprogramming tumor blood vessels for enhancing immunotherapy. *Trends Cancer*. 2017; 3: 809–812. [PubMed: 29198436]
25. Tian L, Goldstein A, Wang H, Ching Lo H, Sun Kim I, Welte T, Sheng K, Dobrolecki LE, Zhang X, Putluri N, Phung TL, et al. Mutual regulation of tumour vessel normalization and immunostimulatory reprogramming. *Nature*. 2017; 544: 250–254. [PubMed: 28371798]
26. Johansson-Percival A, He B, Ganss R. Immunomodulation of tumor vessels: It takes two to tango. *Trends Immunol*. 2018; 39: 801–814. [PubMed: 30153971]
27. Andersen JD, Boylan KL, Jemmerson R, Geller MA, Misemer B, Harrington KM, Weivoda S, Witthuhn BA, Argenta P, Vogel RI, Skubitz AP. Leucine-rich alpha-2-glycoprotein-1 is upregulated in sera and tumors of ovarian cancer patients. *J Ovarian Res*. 2010; 3: 21. [PubMed: 20831812]
28. Sandanayake NS, Sinclair J, Andreola F, Chapman MH, Xue A, Webster GJ, Clarkson A, Gill A, Norton ID, Smith RC, Timms JF, et al. A combination of serum leucine-rich alpha-2-glycoprotein 1, CA19-9 and interleukin-6 differentiate biliary tract cancer from benign biliary strictures. *Br J Cancer*. 2011; 105: 1370–1378. [PubMed: 21970875]
29. Ladd JJ, Busald T, Johnson MM, Zhang Q, Pitteri SJ, Wang H, Brenner DE, Lampe PD, Kucherlapati R, Feng Z, Prentice RL, et al. Increased plasma levels of the APC-interacting protein MAPRE1, LRG1, and IGFBP2 preceding a diagnosis of colorectal cancer in women. *Cancer Prev Res (Phila)*. 2012; 5: 655–64. [PubMed: 22277732]

30. Wu J, Xie X, Nie S, Buckanovich RJ, Lubman DM. Altered expression of sialylated glycoproteins in ovarian cancer sera using lectin-based ELISA assay and quantitative glycoproteomics analysis. *J Proteome Res.* 2013; 12: 3342–3352. [PubMed: 23731285]
31. Wen SY, Zhang LN, Yang XM, Zhang YL, Ma L, Ge QL, Jiang SH, Zhu XL, Xu W, Ding WJ, Yang BQ, et al. LRG1 is an independent prognostic factor for endometrial carcinoma. *Tumour Biol.* 2014; 35: 7125–7133. [PubMed: 24760273]
32. Wang CH, Li M, Liu LL, Zhou RY, Fu J, Zhang CZ, Yun JP. LRG1 expression indicates unfavorable clinical outcome in hepatocellular carcinoma. *Oncotarget.* 2015; 6: 42118–42129. [PubMed: 26517349]
33. Sun DC, Shi Y, Wang LX, Lv Y, Han QL, Wang ZK, Dai GH. Leucine-rich alpha-2-glycoprotein-1, relevant with microvessel density, is an independent survival prognostic factor for stage III colorectal cancer patients: a retrospective analysis. *Oncotarget.* 2017; 8: 66550–66558. [PubMed: 29029535]
34. Yamamoto M, Takahashi T, Serada S, Sugase T, Tanaka K, Miyazaki Y, Makino T, Kurokawa Y, Yamasaki M, Nakajima K, Takiguchi S, et al. Overexpression of leucine-rich alpha2-glycoprotein-1 is a prognostic marker and enhances tumor migration in gastric cancer. *Cancer Sci.* 2017; 108: 2052–2060. [PubMed: 28746773]
35. Zhang Q, Huang R, Tang Q, Yu Y, Huang Q, Chen Y, Wang G, Wang X. Leucine-rich alpha-2-glycoprotein-1 is up-regulated in colorectal cancer and is a tumor promoter. *Onco Targets Ther.* 2018; 11: 2745–2752. [PubMed: 29785123]
36. Wang Y, Xing Q, Chen X, Wang J, Guan S, Chen X, Sun P, Wang M, Cheng Y. The Clinical Prognostic Value of LRG1 in Esophageal Squamous Cell Carcinoma. *Curr Cancer Drug Targets.* 2019; 19: 756–763. [PubMed: 30714525]
37. Guldvik IJ, Zuber V, Braadland PR, Grytli HH, Ramberg H, Lilleby W, Thiede B, Zucknick M, Saatcioglu F, Gislefoss R, Kvåle R, et al. Identification and Validation of Leucine-rich alpha-2-glycoprotein 1 as a Noninvasive Biomarker for Improved Precision in Prostate Cancer Risk Stratification. *Eur Urol Open Sci.* 2020; 21: 51–60. [PubMed: 34337468]
38. Jin Z, Kobayashi S, Gotoh K, Takahashi T, Eguchi H, Naka T, Mori M, Doki Y. The Prognostic Impact of Leucine-Rich alpha-2-Glycoprotein-1 in Cholangiocarcinoma and Its Association With the IL-6/TGF- β 1 Axis. *J Surg Res.* 2020; 252: 147–155. [PubMed: 32278969]
39. Zhang YS, Han L, Yang C, Liu YJ, Zhang XM. Prognostic Value of LRG1 in Breast Cancer: A Retrospective Study. *Oncol Res Treat.* 2021; 44: 36–42. [PubMed: 33242858]
40. Gopinathan A, Morton JP, Jodrell DI, Sansom OJ. GEMMs as preclinical models for testing pancreatic cancer therapies. *Dis Model Mech.* 2015; 8: 1185–1200. [PubMed: 26438692]
41. Gerhardt H, Betsholtz C. Endothelial-pericyte interactions in angiogenesis. *Cell Tissue Res.* 2003; 314: 15–23. [PubMed: 12883993]
42. De Bock K, Cauwenberghs S, Carmeliet P. Vessel abnormalization: another hallmark of cancer? Molecular mechanisms and therapeutic implications. *Curr Opin Genet Dev.* 2011; 21: 73–79. [PubMed: 21106363]
43. Hashizume H, Baluk P, Morikawa S, McLean JW, Thurston G, Roberge S, Jain RK, McDonald DM. Openings between defective endothelial cells explain tumor vessel leakiness. *Am J Pathol.* 2000; 156: 1363–1380. [PubMed: 10751361]
44. Kallenberg D, Tripathi V, Javaid F, Pilotti C, George J, Davis S, Blackburn JWD, O'Connor M, Dowsett L, Bowers CE, Liyanage S, et al. A humanized antibody against LRG1 that inhibits angiogenesis and reduces retinal vascular leakage. *bioRxiv.* 2020; 2020.07.25.218149 doi: 10.1101/2020.07.25.218149
45. Giannotta M, Trani M, Dejana E. VE-cadherin and endothelial adherens junctions: active guardians of vascular integrity. *Dev Cell.* 2013; 26: 441–454. [PubMed: 24044891]
46. Li X, Kumar A, Carmeliet P. Metabolic pathways fueling the endothelial cell drive. *Annu Rev Physiol.* 2019; 81: 483–503. [PubMed: 30742787]
47. Schoors S, De Bock K, Cantelmo AR, Georgiadou M, Ghesquière B, Cauwenberghs S, Kuchnio A, Wong BW, Quaegebeur A, Goveia J, Bifari F, et al. Partial and transient reduction of glycolysis by PFKFB3 blockade reduces pathological angiogenesis. *Cell Metab.* 2014; 19: 37–48. [PubMed: 24332967]

48. Watson HA, Dolton G, Ohme J, Ladell K, Vigar M, Wehenkel S, Hindley J, Mohammed RN, Miners K, Luckwell RA, Price DA, et al. Purity of transferred CD8(+) T cells is crucial for safety and efficacy of combinatorial tumor immunotherapy in the absence of SHP-1. *Immunol Cell Biol.* 2016; 94: 802–808. [PubMed: 27430370]
49. Bertrand F, Montfort A, Marcheteau E, Imbert C, Gilhodes J, Filleron T, Rochaix P, Andrieu-Abadie N, Levade T, Meyer N, Colacios C, et al. TNF α blockade overcomes resistance to anti-PD-1 in experimental melanoma. *Nat Commun.* 2017; 8: 2256 [PubMed: 29273790]
50. Li HY, McSharry M, Bullock B, Nguyen TT, Kwak J, Poczobutt JM, Sippel TR, Heasley LE, Weiser-Evans MC, Clambey ET, Nemenoff RA. The Tumor Microenvironment Regulates Sensitivity of Murine Lung Tumors to PD-1/PD-L1 Antibody Blockade. *Cancer Immunol Res.* 2017; 9: 767–777.
51. Lin H, Wei S, Hurt EM, Green MD, Zhao L, Vatan L, Szeliga W, Herbst R, Harms PW, Fecher LA, Vats P, et al. Host expression of PD-L1 determines efficacy of PD-L1 pathway blockade-mediated tumor regression. *J Clin Invest.* 2018; 128: 805–815. [PubMed: 29337305]
52. Allen E, Missiaen R, Bergers G. Therapeutic induction of high endothelial venules (HEVs) to enhance T-cell infiltration in tumors. *Oncotarget.* 2017; 8: 99207–99208. [PubMed: 29245888]
53. Shirai R, Hirano F, Ohkura N, Ikeda K, Inoue S. Up-regulation of the expression of leucine-rich alpha(2)-glycoprotein in hepatocytes by the mediators of acute-phase response. *Biochem Biophys Res Commun.* 2009; 382: 776–779. [PubMed: 19324010]
54. Liu C, Yen Teo MH, Ting Pek SL, Wu X, Leong ML, Tay HM, Hou HW, Ruedl C, Moss SE, Greenwood J, Tavintharan S, et al. A multifunctional role of leucine-rich-alpha 2 glycoprotein 1 in cutaneous wound healing under normal and diabetic conditions. *Diabetes.* 2020; 69: 2467–2480. [PubMed: 32887674]
55. Gao Y, Xie Z, Ho C, Wang J, Li Q, Zhang Y, Zhou J. LRG1 Promotes Keratinocyte Migration and Wound Repair through Regulation of HIF-1 α Stability. *J Invest Dermatol.* 2020; 140: 455–464. e458 [PubMed: 31344385]
56. Bergers G, Song S. The role of pericytes in blood-vessel formation and maintenance. *Neuro Oncol.* 2005; 7: 452–464. [PubMed: 16212810]
57. Dekker RJ, Boon RA, Rondaij MG, Kragt A, Volger OL, Elderkamp YW, Meijers JC, Voorberg J, Pannekoek H, Horrevoets AJ. KLF2 provokes a gene expression pattern that establishes functional quiescent differentiation of the endothelium. *Blood.* 2006; 107: 4354–4363. [PubMed: 16455954]
58. Egorova AD, Van der Heiden K, Van de Pas S, Vennemann P, Poelma C, DeRuiter MC, Goumans MJ, Gittenberger-de Groot AC, ten Dijke P, Poelmann RE, Hierck BP. Tgfb β /Alk5 signaling is required for shear stress induced klf2 expression in embryonic endothelial cells. *Dev Dyn.* 2011; 240: 1670–1680. [PubMed: 21604321]
59. Park BV, Freeman ZT, Ghasemzadeh A, Chattergoon MA, Rutebemberwa A, Steigner J, Winter ME, Huynh TV, Sebald SM, Lee SJ, Pan F, et al. TGF β 1-Mediated SMAD3 Enhances PD-1 Expression on Antigen-Specific T Cells in Cancer. *Cancer Discov.* 2016; 6: 1366–1381. [PubMed: 27683557]
60. Tang PM, Zhou S, Meng XM, Wang QM, Li CJ, Lian GY, Huang XR, Tang YJ, Guan XY, Yan BP, To KF, et al. Smad3 promotes cancer progression by inhibiting E4BP4-mediated NK cell development. *Nat Commun.* 2017; 8: 14677 [PubMed: 28262747]
61. Zeng Q, Li S, Chepeha DB, Giordano TJ, Li J, Zhang H, Polverini PJ, Nor J, Kitajewski J, Wang CY. Crosstalk between tumor and endothelial cells promotes tumor angiogenesis by MAPK activation of Notch signaling. *Cancer Cell.* 2005; 8: 13–23. [PubMed: 16023595]
62. Graeber TG, Osmanian C, Jacks T, Housman DE, Koch CJ, Lowe SW, Giaccia AJ. Hypoxia-mediated selection of cells with diminished apoptotic potential in solid tumours. *Nature.* 1996; 379: 88–91. [PubMed: 8538748]
63. Anderson AR, Weaver AM, Cummings PT, Quaranta V. Tumor morphology and phenotypic evolution driven by selective pressure from the microenvironment. *Cell.* 2006; 127: 905–915. [PubMed: 17129778]
64. McIntyre A, Harris AL. Metabolic and hypoxic adaptation to anti-angiogenic therapy: a target for induced essentiality. *EMBO Mol Med.* 2015; 7: 368–379. [PubMed: 25700172]

65. Terry S, Faouzi Zaarour R, Hassan Venkatesh G, Francis A, El-Sayed W, Buart S, Bravo P, Thiery J, Chouaib S. Role of hypoxic stress in regulating tumor immunogenicity, resistance and plasticity. *Int J Mol Sci.* 2018; 19 3044 [PubMed: 30301213]
66. Xie ZB, Zhang YF, Jin C, Mao YS, Fu DL. LRG-1 promotes pancreatic cancer growth and metastasis via modulation of the EGFR/p38 signaling. *J Exp Clin Cancer Res.* 2019; 38: 75. [PubMed: 30760292]
67. Takemoto N, Serada S, Fujimoto M, Honda H, Ohkawara T, Takahashi T, Nomura S, Inohara H, Naka T. Leucine-rich α -2-glycoprotein promotes TGF β 1-mediated growth suppression in the Lewis lung carcinoma cell lines. *Oncotarget.* 2015; 6: 11009–11022. [PubMed: 25826092]
68. Singhal M, Gengenbacher N, Pari AAA, Kamiyama M, Hai L, Kuhn BJ, Kallenberg DM, Kulkarni SR, Camilli C, Preu SF, Leuchs B, et al. Temporal multi-omics identifies LRG1 as a vascular niche instructor of metastasis. *Sci Trans Med.* 2021; Sep. 13 (609) eabe6805 doi: 10.1126/scitranslmed.abe6805
69. Kwan YP, Teo MHY, Lim JCW, Tan MS, Rosellinny G, Wahli W, Wang X. LRG1 Promotes Metastatic Dissemination of Melanoma through Regulating EGFR/STAT3 Signalling. *Cancers (Basel).* 2021; 13 3279 [PubMed: 34208965]
70. Wohlkoenig C, Leithner K, Deutsch A, Hrzenjak A, Olschewski A, Olschewski H. Hypoxia-induced cisplatin resistance is reversible and growth rate independent in lung cancer cells. *Cancer Lett.* 2011; 308: 134–143. [PubMed: 21669489]
71. Watson HA, Durairaj RRP, Ohme J, Alatsatianos M, Almutairi H, Mohammed RN, Vigar M, Reed SG, Paisey SJ, Marshall C, Gallimore A, et al. L-selectin enhanced T cells improve the efficacy of cancer immunotherapy. *Front Immunol.* 2019; 10 1321 [PubMed: 31249570]
72. Shrimali RK, Yu Z, Theoret MR, Chinnasamy D, Restifo NP, Rosenberg SA. Antiangiogenic agents can increase lymphocyte infiltration into tumor and enhance the effectiveness of adoptive immunotherapy of cancer. *Cancer Res.* 2010; 70: 6171–6180. [PubMed: 20631075]
73. Slaney CY, Kershaw MH, Darcy PK. Trafficking of T cells into tumors. *Cancer Res.* 2014; 74: 7168–7174. [PubMed: 25477332]
74. Ager A, Watson HA, Wehenkel SC, Mohammed RN. Homing to solid cancers: a vascular checkpoint in adoptive cell therapy using CAR T-cells. *Biochem Soc Trans.* 2016; 44: 377–385. [PubMed: 27068943]
75. Zou W, Wolchok JD, Chen L. PD-L1 (B7-H1) and PD-1 pathway blockade for cancer therapy: Mechanisms, response biomarkers, and combinations. *Sci Transl Med.* 2016; 8 328rv4
76. Galon J, Bruni D. Approaches to treat immune hot, altered and cold tumours with combination immunotherapies. *Nat Rev Drug Discov.* 2019; 18: 197–218. [PubMed: 30610226]
77. O'Donnell JS, Teng MW, Smyth MJ. Cancer immunoediting and resistance to T cell-based immunotherapy. *Nat Rev Clin Oncol.* 2018; 16: 151–167.
78. Griffioen AW, Damen CA, Blijham GH, Groenewegen G. Tumor angiogenesis is accompanied by a decreased inflammatory response of tumor-associated endothelium. *Blood.* 1996; 88: 667–673. [PubMed: 8695814]
79. Griffioen AW, Damen CA, Martinotti S, Blijham GH, Groenewegen G. Endothelial intercellular adhesion molecule-1 expression is suppressed in human malignancies: the role of angiogenic factors. *Cancer Res.* 1996; 56: 1111–1117. [PubMed: 8640769]
80. Piali L, Fichtel A, Terpe HJ, Imhof BA, Gisler RH. Endothelial vascular cell adhesion molecule 1 expression is suppressed by melanoma and carcinoma. *J Exp Med.* 1995; 181: 811–816. [PubMed: 7530765]
81. Joyce JA, Fearon DT. T cell exclusion, immune privilege, and the tumor microenvironment. *Science.* 2015; 348: 74–80. [PubMed: 25838376]
82. Klein D. The tumor vascular endothelium as decision maker in cancer therapy. *Front Oncol.* 2018; 8: 367. [PubMed: 30250827]
83. Tual-Chalot S, Garcia-Collado M, Redgrave RE, Singh E, Davison B, Park C, Lin H, Luli S, Jin Y, Wang Y, Lawrie A, et al. Loss of endothelial endoglin promotes high-output heart failure through peripheral arteriovenous shunting driven by VEGF signaling. *Circ Res.* 2020; 126: 243–257. [PubMed: 31805812]

84. Moser AR, Luongo C, Gould KA, McNeley MK, Shoemaker AR, Dove WF. ApcMin: a mouse model for intestinal and mammary tumorigenesis. *Eur J Cancer*. 1995; 31A: 1061–1064. [PubMed: 7576992]
85. Hingorani SR, Wang L, Multani AS, Combs C, Deramaudt TB, Hruban RH, Rustgi AK, Chang S, Tuveson DA. Trp53R172H and KrasG12D cooperate to promote chromosomal instability and widely metastatic pancreatic ductal adenocarcinoma in mice. *Cancer Cell*. 2005; 7: 469–483. [PubMed: 15894267]
86. el Marjou F, Janssen KP, Chang BH, Li M, Hindie V, Chan L, Louvard D, Chambon P, Metzger D, Robine S. Tissue-specific and inducible Cre-mediated recombination in the gut epithelium. *Genesis*. 2004; 39: 186–193. [PubMed: 15282745]
87. Shibata H, Toyama K, Shioya H, Ito M, Hirota M, Hasegawa S, Matsumoto H, Takano H, Akiyama T, Toyoshima K, Kanamaru R, et al. Rapid colorectal adenoma formation initiated by conditional targeting of the Apc gene. *Science*. 1997; 278: 120–123. [PubMed: 9311916]

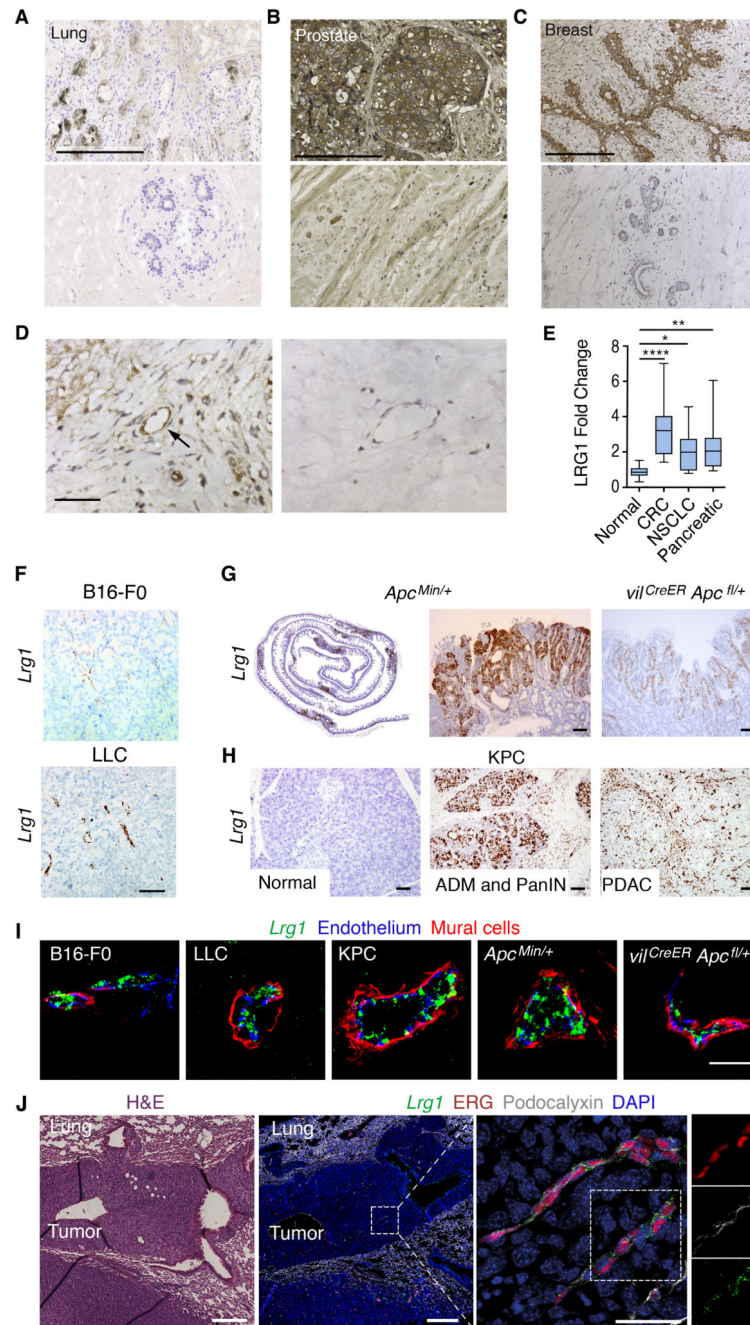


Figure 1. LRG1 is expressed in cancer

(A–C) LRG1 protein expression (brown) in human cancers (A–C, top images) and either normal tissue (A and C) or normal-appearing adjacent tissue (B, bottom images). Lung squamous cell carcinoma (A), (B) prostate adenocarcinoma, and (C) invasive ductal breast carcinoma. Scale bar, 200 μ m.

(D) Higher power images of increased LRG1 expression in vessel (arrow) from peritumoral breast carcinoma (left) compared with normal breast tissue (right). Scale bar, 60 μ m.

(E) Box and whisker plot showing that serum LRG1 is increased, relative to healthy controls, in treatment-naïve patients with colorectal adenocarcinoma (CRC), non-small cell lung carcinoma (NSCLC: squamous cell carcinoma), and pancreatic adenocarcinoma (n = 15 per group). Kruskal-Wallis with Dunn post-test. Boxes extend from the 25th to the 75th percentile. Whiskers represent the minimum and maximum data points. *p < 0.05, **p < 0.01, ***p < 0.0001.

(F–H) *Lrg1* transcript expression in (F) B16-F0 and LLC syngeneic subcutaneous mouse tumors, (G) small intestine (left image, intestine roll) of genetically engineered mouse cancer models *Apc^{Min/+}* and *vil^{CreER} Apc^{fl/+}*, and (H) normal or diseased pancreas showing acinar ductal carcinoma (ADM), pancreatic intraepithelial neoplasia (PanIN), or PDAC from KPC mice. Scale bar, 50 µm.

(I) Vascular *Lrg1* transcript expression (green) and immunohistochemical cell markers for endothelium (CD31; blue) and mural cells (α-SMA; red) in mouse primary tumors. Scale bar, 30 µm.

(J) Histological section through LLC lung metastasis and adjacent section labeled for *Lrg1* transcript (green) and endothelial cell markers ERG (red) and podocalyxin (white). Enlarged area shows tumor vessels expressing *Lrg1* transcript. Low-magnification scale bar, 250 µm. High-magnification scale bar, 50 µm.

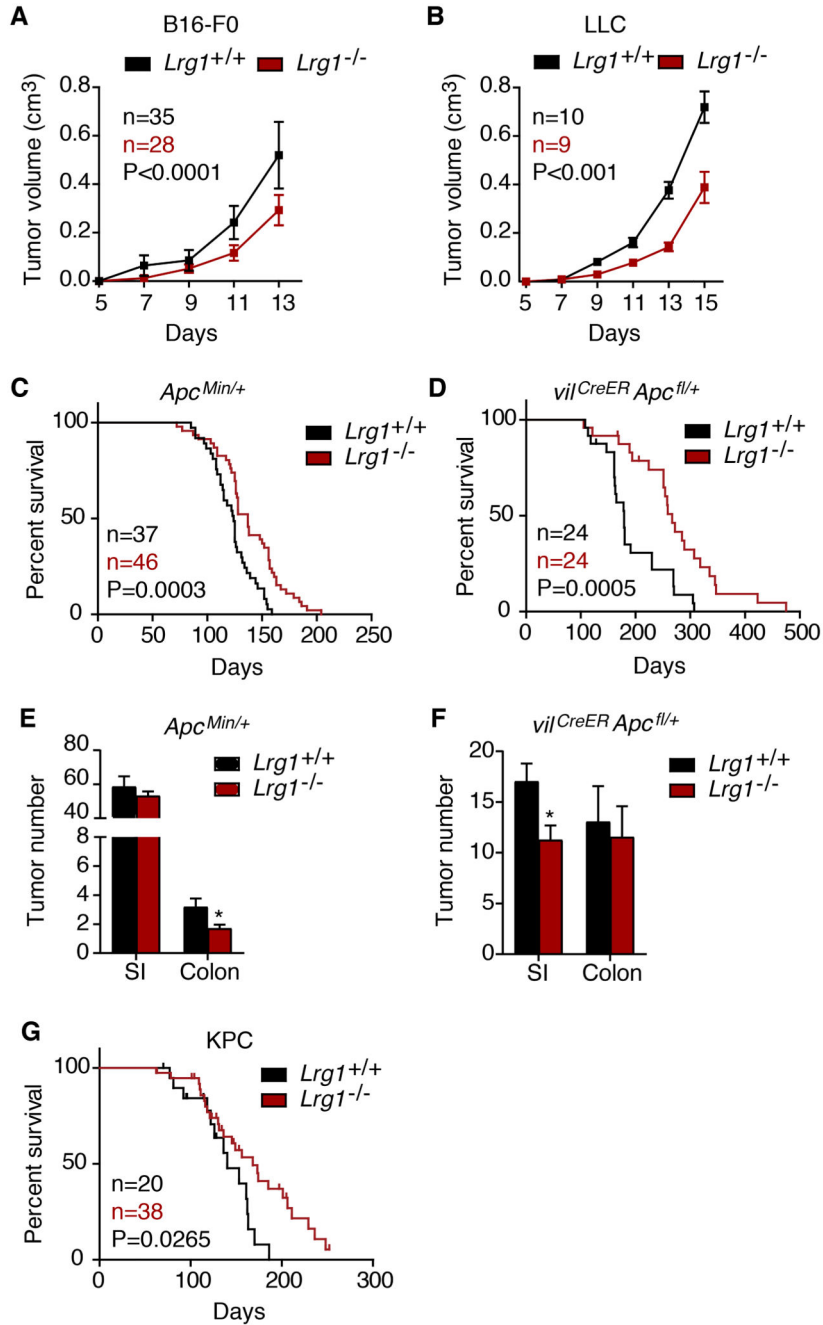


Figure 2. *Lrg1* deletion reduces tumor volume and enhances survival

(A and B) Growth curves of (A) B16-F0 and (B) LLC subcutaneous tumors in *Lrg1*^{+/+} and *Lrg1*^{-/-} mice (mean ± 95% confidence interval [CI]). Repeated-measures 2-way ANOVA.

(C and D) Kaplan-Meier curve of *Apc*^{Min/+} (C) and *vil*^{CreER} *Apc*^{fl/+} mice with or without homozygous deletion of *Lrg1*. Mantel-Cox test.

(E and F) Tumor number in *Apc*^{Min/+} (n = 16 *Lrg1*^{+/+} and n = 27 *Lrg1*^{-/-}) and *vil*^{CreER} *Apc*^{fl/+} (n = 11 *Lrg1*^{+/+} and n = 11 *Lrg1*^{-/-}) mouse small intestine (SI) and colon with or without homozygous deletion of *Lrg1*. Mean ± 95% CI. Mann-Whitney, *p < 0.05. (G)

Kaplan-Meier curve of KPC mice with or without homozygous deletion of *Lrg1*. Mantel-Cox test.

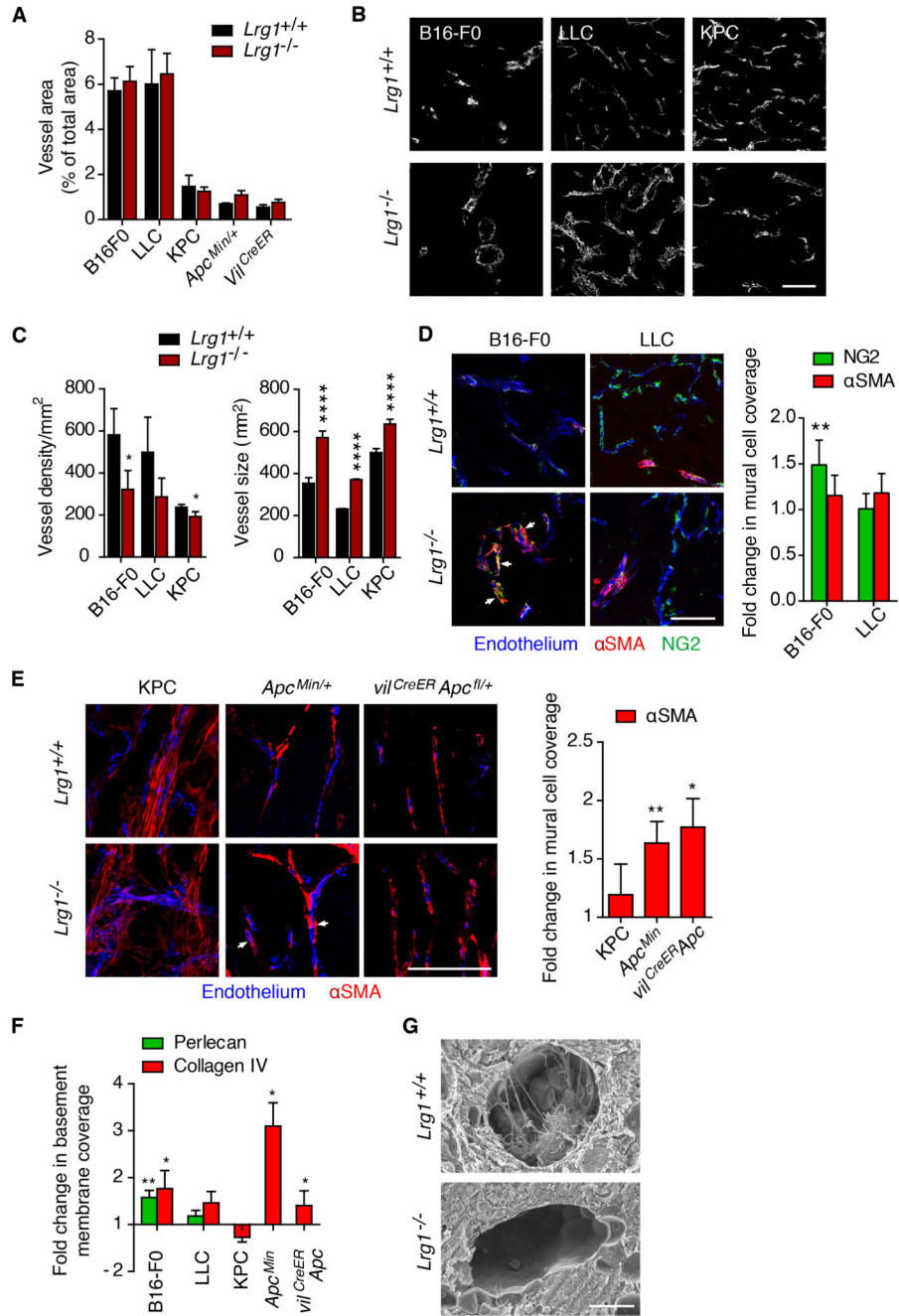


Figure 3. *Lrg1* deletion affects vascular structure

(A) Vessel area for different tumors expressed as the percentage of field that was positive for the endothelial cell marker CD31. Mean \pm 95% CI. (B and C) Representative images (from $n > 3$) of CD31 stained sections of the vasculature from B16-F0, LLC, and KPC tumors from *Lrg1*^{+/+} and *Lrg1*^{-/-} mice (scale bar, 50 μ m) (B), and (C) quantification of vessel density and size (cross-sectional area) of individual CD31⁺ vessels. B16-F0 tumors ($n = 15$ *Lrg1*^{+/+} and $n = 17$ *Lrg1*^{-/-}), LLC tumors ($n = 28$ *Lrg1*^{+/+} and $n = 25$ *Lrg1*^{-/-}), and KPC tumors ($n = 15$ *Lrg1*^{+/+} and $n = 15$ *Lrg1*^{-/-}) were analyzed. (D) Representative images (from $n > 3$) of immunofluorescence staining for Endothelium (blue), α SMA (red), and NG2 (green) in B16-F0 and LLC tumors from *Lrg1*^{+/+} and *Lrg1*^{-/-} mice (scale bar, 50 μ m). (E) Representative images (from $n > 3$) of immunofluorescence staining for Endothelium (blue) and α SMA (red) in KPC, *Apc*^{Min/+}, and *Vil*^{CreER} *Apc*^{fl/+} tumors from *Lrg1*^{+/+} and *Lrg1*^{-/-} mice (scale bar, 50 μ m). (F) Representative images (from $n > 3$) of immunofluorescence staining for Perlecan (green) and Collagen IV (red) in B16-F0, LLC, KPC, *Apc*^{Min}, and *Vil*^{CreER} *Apc* tumors from *Lrg1*^{+/+} and *Lrg1*^{-/-} mice (scale bar, 50 μ m). (G) Electron micrographs of *Lrg1*^{+/+} and *Lrg1*^{-/-} vessels (scale bar, 500 nm).

= 7 *LrgI*^{+/+} and n = 10 *LrgI*^{-/-}). Mean ± 95% CI; Mann-Whitney, with no corrections for multiple testing, *p < 0.05, ****p < 0.0001.

(D) Mural cell (NG2 or a-SMA) association with tumor endothelial cell (CD31 or podocalyxin) in B16-F0 and LLC tumors from mice with or without homozygous deletion of *LrgI*. Tight association of NG2⁺ mural cells with the tumor vessel is indicated by arrowheads (scale bar, 100 μm). Mean ± 95% CI. Student's t test, **p < 0.01.

(E) Mural cell (a-SMA) association with tumor endothelial cell (CD31) from KPC, *Apc*^{Min/+}, and *viCreER Apc*^{fl/+} tumor models in wild-type and *LrgI* null mice. Tight association of a-SMA⁺ mural cells with the tumor vessel is indicated by arrowheads. For NG2, B16-F0 (n = 10 *LrgI*^{+/+} and n = 15 *LrgI*^{-/-} mice) and LLC (n = 14 *LrgI*^{+/+} and n = 15 *LrgI*^{-/-} mice). For a-SMA, B16-F0 (n = 11 *LrgI*^{+/+} and n = 15 *LrgI*^{-/-} mice), LLC (n = 7 *LrgI*^{+/+} and n = 7 *LrgI*^{-/-} mice), KPC (n = 5 *LrgI*^{+/+} and n = 10 *LrgI*^{-/-} mice), and *Apc*^{Min/+} (mean values from n = 8 *LrgI*^{+/+} and n = 11 *LrgI*^{-/-} mice). Scale bars, 100 μm. Mean ± 95% CI. Student's t test. *p < 0.05, **p < 0.01.

(F) Endothelial basement membrane (perlecan and/or collagen IV) association with tumor endothelium (CD31). For perlecan, B16-F0 (n = 12 *LrgI*^{+/+} and n = 11 *LrgI*^{-/-} mice) and LLC (n = 19 *LrgI*^{+/+} and n = 18 *LrgI*^{-/-} mice). For collagen IV, B16-F0 (n = 12 *LrgI*^{+/+} and n = 11 *LrgI*^{-/-} mice), LLC (n = 19 *LrgI*^{+/+} and n = 18 *LrgI*^{-/-} mice), KPC (n = 4 *LrgI*^{+/+} and n = 8 *LrgI*^{-/-} mice), and *Apc*^{Min/+} (mean per mouse, n = 5 *LrgI*^{+/+} and n = 10 *LrgI*^{-/-} mice); Mean ± 95% CI. Mann-Whitney, *p < 0.05, **p < 0.01.

(G) Scanning electron microscopy of blood vessels in B16-F0 tumors grown in *LrgI*^{+/+} or *LrgI*^{-/-} mice. Scale bar, 5 μm.

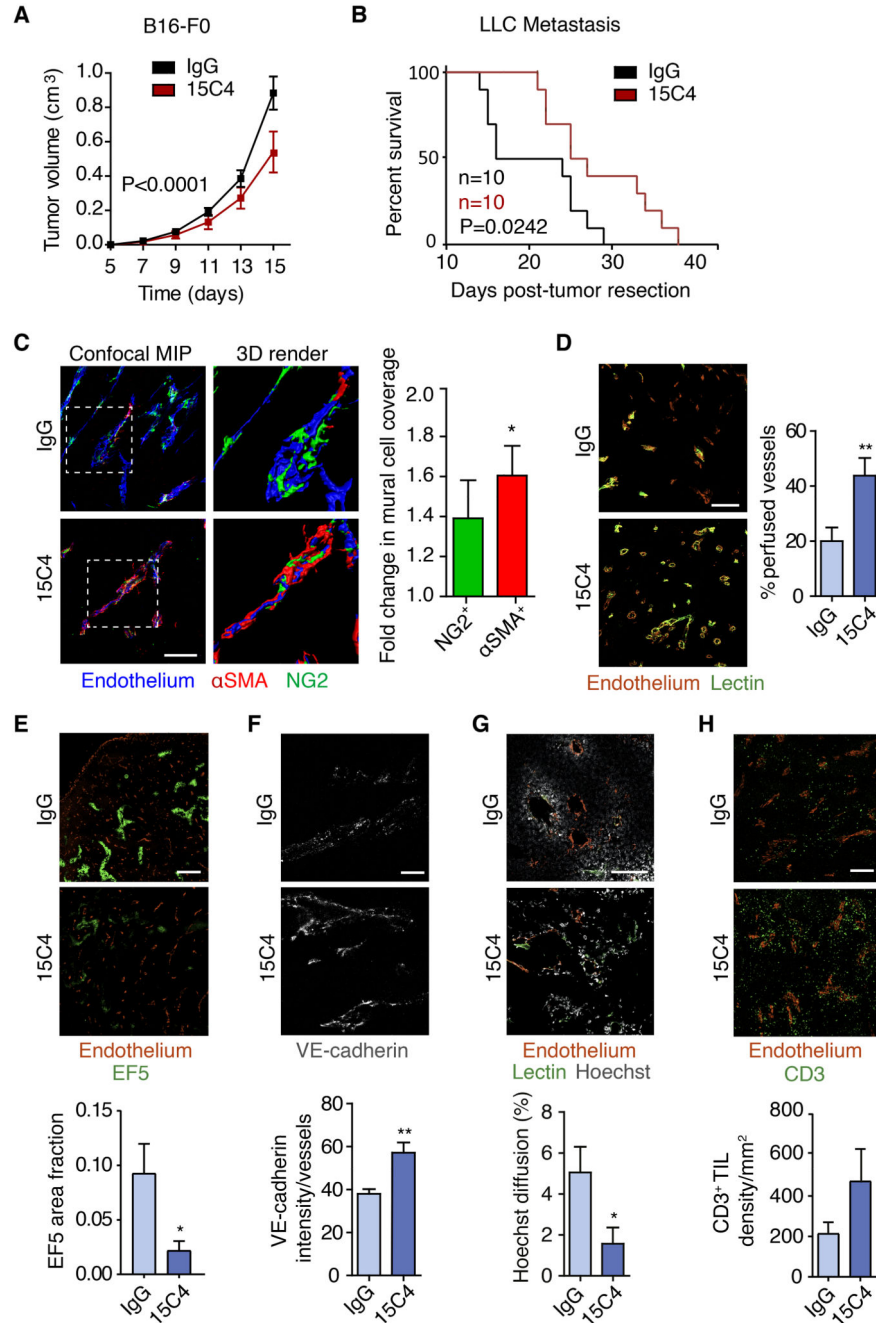


Figure 4. Antibody inhibition of LRG1 inhibits primary B16-F0 tumor growth, enhances survival in metastatic cancer, and normalizes tumor vasculature

(A) Mean tumor volumes of B16-F0 tumors from wild-type mice treated with anti-LRG1 (15C4) or control antibody (IgG) (mean ± 95% CI). IgG, n = 35 mice; 15C4, n = 39 mice. Two-way repeated measures ANOVA.

(B) Kaplan-Meier curve showing overall survival of mice after primary subcutaneous LLC tumor resection when treated with control IgG or 15C4 in perioperative setting (n = 10 mice per group; 50 mg/kg twice per week). Mice with primary tumor regrowth were excluded from the analysis. Mantel-Cox test.

(C) Immunohistochemistry and quantification of mural cell (NG2 and α -SMA) association with B16-F0 tumor endothelium (CD31 or podocalyxin) from wild-type mice treated with anti-LRG1 (15C4) or control antibody (IgG). Scale bar, 100 μ m. 3D renders of the highlighted areas are shown. Graph shows fold change (mean \pm SEM) in mural cell overlap. For NG2, IgG n = 11, 15C4 n = 12. For α -SMA, IgG n = 16, 15C4 n = 19 tumors. Student's t test. *p < 0.05.

(D–H) Immunohistochemistry and quantification of (D) tumor vessel perfusion (lectin; n = 12 tumors per condition; scale bar, 200 μ m), (E) hypoxia (EF5; IgG, n = 7; 15C4, n = 5 tumors; scale bar, 1 mm), (F) adherens junction molecule (VE-cadherin; n = 5 tumors per condition; scale bar, 50 μ m), (G) permeability (Hoechst; IgG, n = 11; 15C4, n = 10 tumors; scale bar, 200 μ m), and (H) tumor-infiltrated lymphocyte density (CD3+ lymphocytes; IgG, n = 13; 15C4, n = 11 tumors; scale bar, 250 μ m).

For all graphs, means \pm SEMs; Student's t test, *p < 0.05, **p < 0.01.

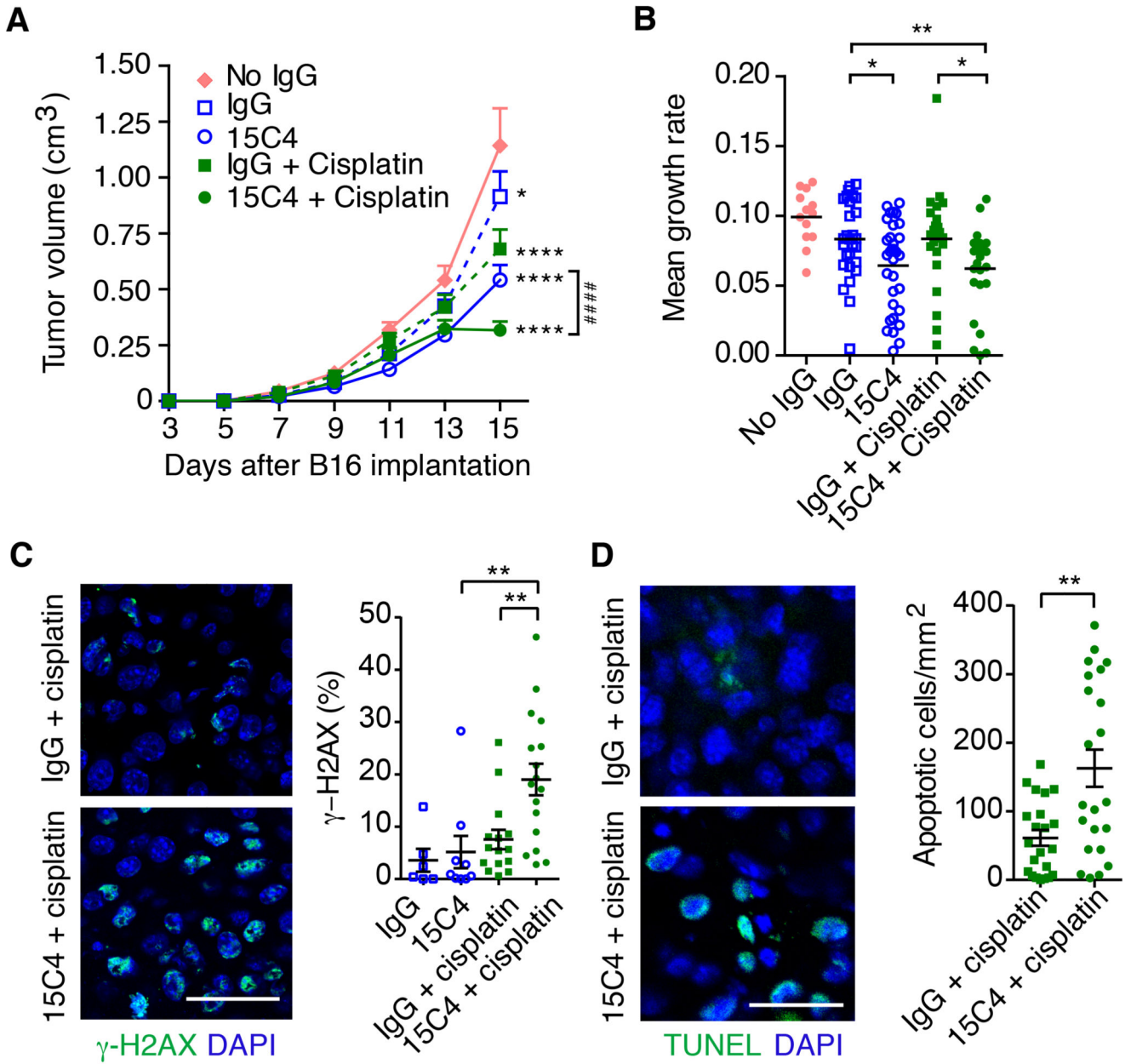


Figure 5. Antibody inhibition of LRG1 enhances the efficacy of cisplatin Treatment of B16-F0 tumors with 15C4 (50 mg/kg) and cisplatin (2.5 mg/kg)

(A) Growth curves (means ± SEMs), analyzed by linear regression comparing to no IgG (* $p < 0.05$, **** $p < 0.0001$) or pairs as shown (#### $p < 0.0001$). No IgG, $n = 13$; IgG, $n = 28$; 15C4, $n = 33$; IgG + cisplatin, $n = 23$ and 15C4 + cisplatin, $n = 27$ mice.

(B) Growth rate (slope) of each tumor. Student's t test, * $p < 0.05$, ** $p < 0.01$.

(C) DNA double-strand breaks detected with antibody against g-H2AX (green). DAPI shown in blue. Scale bar, 30 μm . Graph shows percentage of g-H2AX+ nuclei (mean ± 95% CI). Oneway ANOVA, ** $p < 0.01$. IgG, $n = 6$; 15C4, $n = 9$; IgG + cisplatin, $n = 15$ and 15C4 + cisplatin, $n = 17$ mice.

(D) Apoptotic cells revealed by TUNEL staining (green). DAPI shown in blue. Scale bar, 30 μm . Graph shows density of TUNEL+ apoptotic cells (mean \pm SEM). Student's t test, ** $p < 0.01$. IgG + cisplatin, $n = 22$ and 15C4 + cisplatin, $n = 22$ mice.

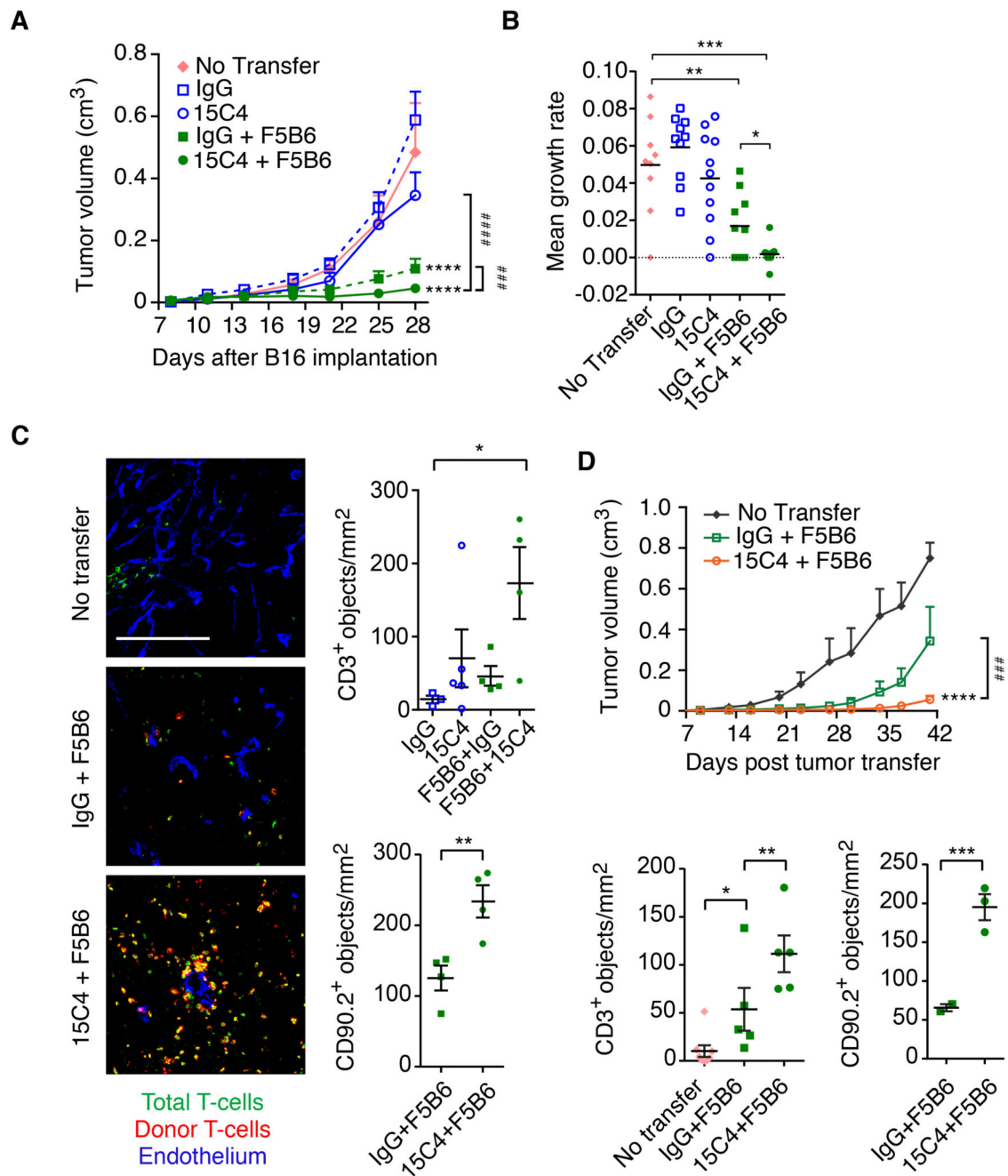


Figure 6. Antibody inhibition of LRG1 improves the efficacy of adoptive T cell therapy

Treatment of mice bearing NP68-expressing B16-F10 subcutaneous tumors with 15C4 and F5B6 cytotoxic T cells.

(A) Growth curves (means \pm SEM), analyzed by linear regression comparing to no transfer (****p < 0.0001) or pairs as shown (###p < 0.001, ####p < 0.0001). No transfer, n = 9; IgG, n = 10; 15C4, n = 11; IgG + F5B6, n = 10 and 15C4 + F5B6, n = 11 mice.

(B) Growth rate (slope) of each tumor. Mean \pm SEM. Student's t test, *p < 0.05, **p < 0.01, ***p < 0.001.

(C) T cell infiltration of tumors taken from animals shown in (A) above. Scale bar, 200 μm . Graphs show density (objects/ mm^2) of CD3⁺ T cells (top) and of CD90.2⁺ donor cells (bottom). Mean \pm SEM. Student's t test, * $p < 0.05$, ** $p < 0.01$.

(D) As in (A), but with reduced F5B6 cytotoxic T cell treatment. Graphs show density (objects/ mm^2) of CD3⁺ T cells (left) and of CD90.2⁺ donor cells (right). No transfer, $n = 8$; IgG + F5B6, $n = 10$; 15C4 + F5B6, $n = 10$. Mean \pm SEM. Linear regression. * $p < 0.05$, ** $p < 0.01$, *** $p < 0.001$.

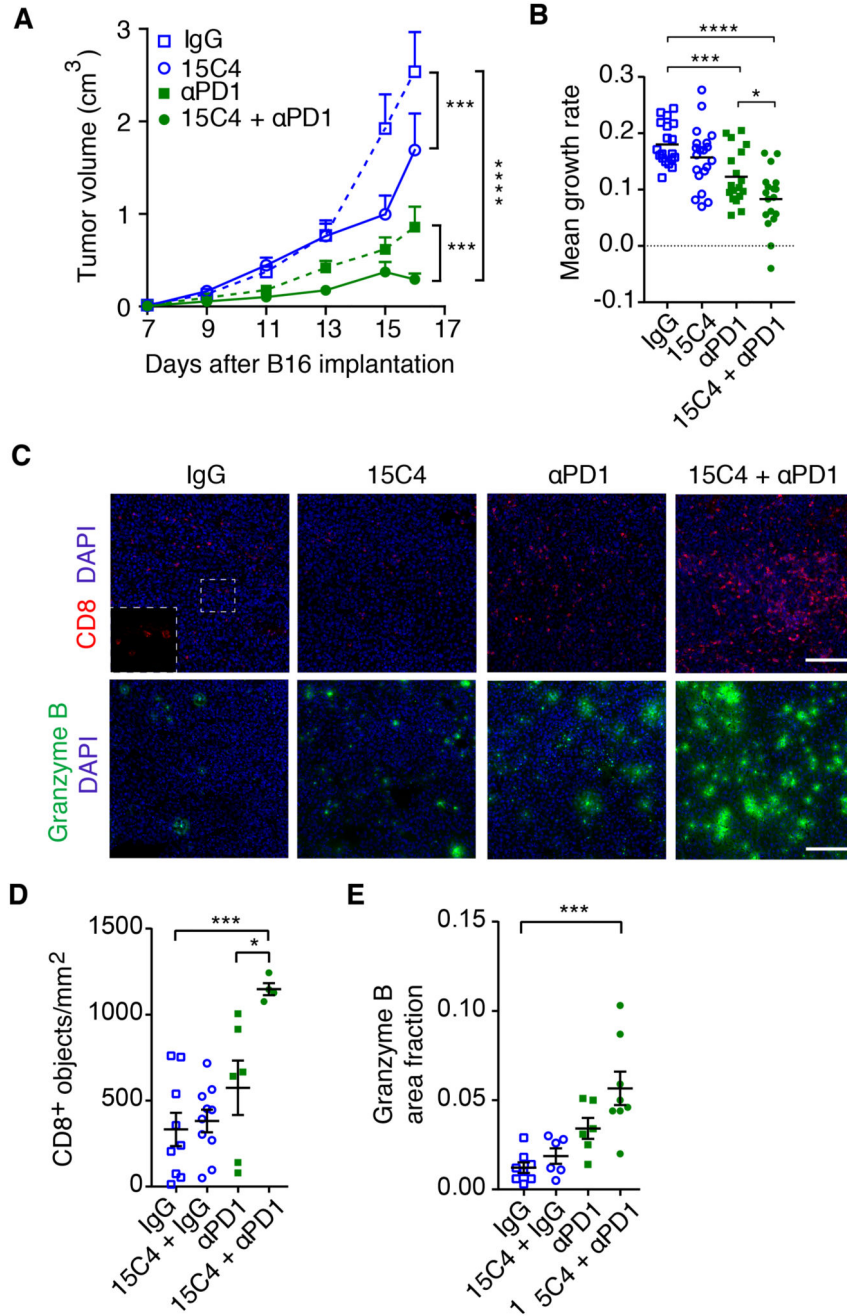


Figure 7. Inhibition of LRG1 with a blocking antibody improves the efficacy of checkpoint inhibition

Treatment of B16-F0 subcutaneous tumors with 15C4 and anti-PD1

(A) Growth curves (means ± SEMs), analyzed by linear regression comparing pairs as shown. ***p < 0.001, ****p < 0.0001. n = 21 tumors per arm.

(B) Growth rate (slope) of each tumor. Mean ± SEM. Student's t test. *p < 0.05, ***p < 0.001, ****p < 0.0001.

(C) CD8⁺ (red) and granzyme B⁺ (green) T cell infiltration of tumors. DAPI shown in blue. Scale bars, 150 μm (top) and 150 μm (bottom).

(D and E) Graphs show density (objects/mm²) of CD8⁺ T cells (D) and granzyme B area fraction

(E). n = 9, 10, 6, and 4 for (D) and n = 8, 6, 6, and 8 for (E) tumors. Mean ± SEM. Student's t test, *p < 0.05, ***p < 0.001.